Contact angles for perfectly wetting pure liquids evaporating into air: Between de Gennes-type and other classical models

A. Ye. Rednikov* and P. Colinet†
Université libre de Bruxelles, TIPs Laboratory, CP 165/67, 1050 Brussels, Belgium

(Received 7 November 2018; accepted 27 October 2020; published 30 November 2020)

The present theoretical study is concerned with evaporation-induced apparent contact angles for a perfectly wetting one-component liquid placed on a flat solid substrate and undergoing diffusion-limited evaporation into ambient air. The analysis pertains to a distinguished small vicinity of the contact line (the "microregion"), where such angles are established and where various microscopic effects typically enable relaxing the well-known evaporation-flux singularity. We proceed from a Joanny-Hervet-de Gennes-type approach, involving the spreading coefficient, disjoining pressure in the form of an inverse cubic law, and a truncated microfilm (precursor film) starting abruptly at a solid surface. A more classical regime with an (infinitely) extended adsorbed microfilm is recovered therefrom in the limit of large spreading coefficients upon additional incorporation of the Kelvin effect (dew point shift due to the liquid–gas pressure difference). The latter regime is critically revisited with a view to clarifying the scaling prefactor known in the literature. The influence of the kinetic resistance to evaporation is analyzed as well.

DOI: 10.1103/PhysRevFluids.5.114007

I. INTRODUCTION

The fact that evaporation can give rise to finite apparent contact angles even for perfectly wetting pure liquids (zero Young's angle) has already been known for quite a while, although it is difficult to be traced back to the original reference. On the one hand, such angles can be seen as a compromise between the tendencies to spread and to evaporate. On the other hand, a key feature is the localization of the zone where they are established near the contact line, rather than being merely smeared over larger scales. This is what makes these angles really *apparent* ones, as seen from those larger scales. Such localization comes as a result of a *macroscopic* singularity of the evaporation flux towards the contact line, also giving rise to liquid flow singularities. Such singularities can only be regularized by means of certain *microscopic* effects (e.g., disjoining pressure, precursor films, Navier slip, kinetic resistance to phase change, Kelvin effect). This happens in a distinguished small vicinity of the contact line, referred to as the *microregion*, where the evaporation-induced apparent contact angles are established. Since it is these angles that we are concerned with here, the present analysis is naturally focused on the microregion, where the problem can be formulated in its own right, ignoring the coupling to any specific macroscopic shape (drop, bubble, meniscus, etc.). The evaporation-induced angles and the associated liquid film slopes in the microregion turn out to be quite small (after all, they must vanish in the limit of weak evaporation for perfectly wetting liquids), so that a thin-film (lubrication) approximation is quite applicable in this context. The typical evaporative microregion problem is steady with the contact line remaining at rest, and it will be

*aredniko@ulb.ac.be
†pcolinet@ulb.ac.be

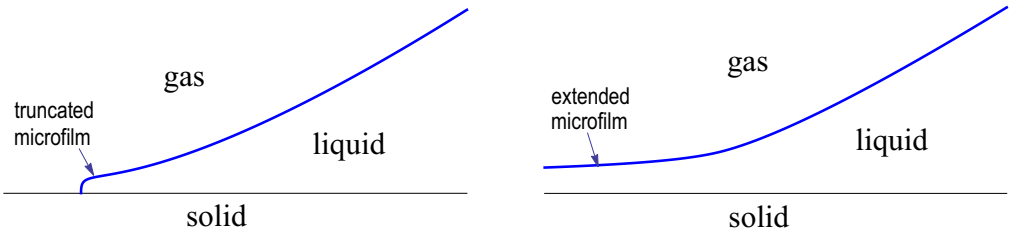

FIG. 1. Sketch of the microregion profiles with truncated and extended microfilms.

considered as such in the present paper, the evaporative losses being compensated by an influx from the macroscopic side of the liquid film. In the cases when the motion of the contact line is nonetheless essential, its effect can then be evaluated by means of the Cox-Voinov relation, the evaporation-induced contact angle taking the place of the Young's angle therein.

While the above general picture does not depend on the nature of the evaporation process, the latter does make a difference as far as finer physical details as well as the mathematical description are concerned. In the literature, there are two large groups of studies in this regard. One of them considers evaporation into an atmosphere composed exclusively of the pure vapor of the liquid involved, with no inert or noncondensable gases [1–21]. In this case, to ensure evaporation, the substrate must be superheated relative to the saturation (boiling) temperature corresponding to the vapor pressure, the later being practically constant [13]. The evaporation rate is limited by heat conduction across the liquid film, compensating for the latent heat of evaporation. This is a situation typical for boiling applications. The other large group of studies deals with diffusion-limited evaporation into a noncondensable gas atmosphere such as air, the total gas pressure being constant and the thermal effects inessential (e.g., Refs. [12,22–29]). For instance, this is the situation for a sessile drop evaporating into ambient air. The present paper belongs to this second group of studies, for which fully-fledged models appeared only in the last decade and to which we limit our attention hereafter.

The microscopic model most classically used in the literature implies an infinitely *extended* adsorbed microfilm, covering all solid surface even far away from the macroscopic portions of the liquid [23,27,28]. Of these works, Refs. [23,27] incorporate the microregion as an inseparable part of a larger, macroscopic problem of an evaporating sessile droplet [23] or meniscus [27], whereas Ref. [28] comes up with a closed-form evaporative microregion problem *per se*, which is most relevant in the context of the present paper. However, ending in such an extended adsorbed microfilm is not the only plausible microregion structure. Another one considered in the literature, of a (Joanny-Hervet-)de Gennes type, involves a *truncated* microfilm (precursor film) abruptly starting at the solid surface (cf. Fig. 1), as elaborated in the static and moving-contact-line contexts in Refs. [30–33] and closer to the present evaporative context in Ref. [12], which differs from the model of Refs. [24–26] principally by the choice of the boundary conditions at the tip of the film.[1] In the present paper, we aim at a unifying view of such different approaches, complementarily revisit the mentioned evaporative microregion models and consider the ones lying in between. We proceed from the de Gennes-type model of Ref. [12] adopted as the basic one here. It is arguably the simplest possible consistent model, with a mathematical formulation incomparably simpler than for other models due to a lucky vapor-diffusion decoupling from the liquid film dynamics. Then, certain pertinent microphysics generalizations are explored (see below), in particular, giving rise to the extended-microfilm model in a limiting case. In this way, we shall eventually establish an

[1]Recently, there were some studies on different drop types (nonvolatile case) where some room was given to the discussion of drops with truncated microfilms [34].

interrelation between these models as well as see how the result for the evaporation-induced angle is affected by such microscopic details.

The only microscopic effect in the present basic de Gennes-type model is the mechanical action of a disjoining pressure in the form of a positive inverse-cubic law $\Pi^* = \gamma^* a^{*2}/h^{*3}$, where γ^* is the gas–liquid interfacial tension, a^* is the molecular length scale (typically in the subnanometric range), and h^* the film thickness. The microfilm being truncated, the spreading coefficient S^* also appears among the parameters of the problem. The scale ϵ of the film slopes dh^*/dx^* in such a microregion (x^* being the Cartesian coordinate along the film), and hence the scale of the evaporation-induced contact angle, is given by (see Sec. 4.2 in Ref. [12])

$$\epsilon = \left(\frac{3^{3/4} \nu_l^* D_g^* \rho_{v,\mathrm{sat}}^*}{\gamma^* a^{*1/2} \ell^{*1/2}} \right)^{1/3}. \tag{1}$$

Here D_g^* is the diffusion coefficient of the vapor in the gas phase; $\nu_l^* = \mu_l^*/\rho_l^*$, μ_l^* and ρ_l^* are the kinematic and dynamic viscosities and density of the liquid, respectively; $\rho_{v,\mathrm{sat}}^* = p_{v,\mathrm{sat}}^* M^*/(R_g^* T^*)$ the saturation density of the vapor, T^* the temperature, $p_{v,\mathrm{sat}}^*$ the saturation pressure at T^*, M^* the molar mass, and R_g^* the universal gas constant. Furthermore, ℓ^* is a length parameter characterizing a given macroscopic configuration. For instance,

$$\ell^* = \tfrac{1}{2}\pi^2 R_c^* \tag{2}$$

for a thin sessile droplet in the diffusion-limited regime of evaporation, where R_c^* is its contact radius. As already mentioned, the evaporation-induced angles are typically small, implying $\epsilon \ll 1$ as we shall assume here. The problem for this basic de Gennes-type model was fully formulated in Ref. [12], although we did not provide the computation results. A first objective of the present paper will then be to fill in this gap. The principal result, for the evaporation-induced contact angle here denoted θ_{mic} (the subscript "mic" intended to convey the idea of a microscopic, or microregion contact angle), is represented in the form

$$\theta_{\mathrm{mic}} = \epsilon\, \vartheta_{\mathrm{mic}}. \tag{3}$$

Here θ_{mic} is the value in radians, whereas ϑ_{mic} is a rescaled value such that generally $\vartheta_{\mathrm{mic}} = O(1)$ while $\epsilon \ll 1$. The prefactor ϑ_{mic} in Eq. (3) is generally a function of the parameters of the problem. For the basic model, it turns out to be only a function of the dimensionless spreading coefficient

$$\Sigma = \frac{2S^* \epsilon^{-2}}{\gamma^*}, \tag{4}$$

i.e., $\vartheta_{\mathrm{mic}} = \vartheta_{\mathrm{mic}}(\Sigma)$ (cf. Ref. [12]). Such a basic model will further be treated in Sec. II below.

For an estimation of typical values, we use $\rho_{v,\mathrm{sat}}^* \sim 0.2\,\mathrm{kg/m^3}$ ($\sim$20% of air density), $\nu_l^* \sim 10^{-6}\,\mathrm{m^2/s}$, $D_g^* \sim 10^{-5}\,\mathrm{m^2/s}$, $\gamma^* \sim 20\,\mathrm{mN/m}$, $a^* \sim 0.3\,\mathrm{nm}$, and $R_c^* \sim 1\,\mathrm{mm}$. Then from Eqs. (1) and (2), we obtain $\epsilon \sim 0.06$, which a sufficiently small value indeed (corresponding to $\sim 3^\circ$). Larger values of ϵ can be obtained for more volatile liquids, characterized by larger $\rho_{v,\mathrm{sat}}^*$.

It is remarkable that the scaling Eqs. (1)–(3) for the evaporation-induced angles, with a prefactor yet to be determined, naturally comes up once van der Waals forces (the disjoining pressure of the form $\Pi^* = \gamma^* a^{*2}/h^{*3}$) are recognized as a key [22,27,29], irrespective of other possible details of a model that would just affect the prefactor. For instance, in Ref. [22], where an equivalent of Eqs. (1)–(3) was put forth apparently for the first time in the literature, it was just a naturally occurring scaling, without delving into further details of the formulation or the feasibility of the latter. In Ref. [29], the results of the model with an extended adsorbed microfilm [28] were rendered in this same scaling. It is important to note at this juncture that to ensure the existence of such a microfilm, the sole mechanical action of the disjoining pressure is not sufficient (whereas it *is* sufficient in the framework of the present basic model with truncated microfilms), and another effect acting at microscopic scales is actually taken into consideration [23,27,28]. Namely, we mean the Kelvin effect. It consists in a saturation point shift caused by a pressure difference between the liquid and

the vapor, most notably due to the Laplace and disjoining pressures, hence in particular amounting to a thermodynamic action of the disjoining pressure rendering possible a local thermodynamic equilibrium between an adsorbed microfilm and the vapor. Thus, there must be a kind of Kelvin number Ke (to be defined later on in Sec. IV) appearing in the model[2]. In contrast, Σ does not appear since there is no three-phase contact line (the extended microfilm covering all the surface), hence $\vartheta_{\rm mic} = \vartheta_{\rm mic}({\rm Ke})$ in Eq. (3). However, if the Kelvin effect is incorporated into the present basic model with truncated microfilms, which we shall do in Sec. IV, then we will arrive at $\vartheta_{\rm mic} = \vartheta_{\rm mic}(\Sigma, {\rm Ke})$, the basic model being recovered at ${\rm Ke} = 0$.

Here comes another objective of the present paper to be also fulfilled in Sec. IV. Similar to the program we accomplished in Ref. [11] in the case of evaporation into the pure vapor, but here for a very distinct case of diffusion-limited evaporation into air (hence anticipating no full analogy), we shall show that the microregion regime with an extended microfilm is a limiting case in the family of truncated-microfilm regimes at $\Sigma \gg 1$ (provided the Kelvin effect *is* incorporated).

Then, as an important by-product of the study, such a limit will also permit us to obtain the prefactor $\vartheta_{\rm mic}({\rm Ke})$ in the *extended*-microfilm regime. The latter result could be expected to coincide with Ref. [28] (cf. also the representation thereof given in Ref. [29]). Nonetheless, $\vartheta_{\rm mic}({\rm Ke})$ was calculated in Ref. [28] by asymptotic means in the limit of small Kelvin numbers (speaking in our terms) and may differ from the corresponding numerical result. Therefore, we shall here also undertake a direct numerical computation of the more classical, extended-microfilm problem to see whether we obtain the same result for $\vartheta_{\rm mic}({\rm Ke})$ in the mentioned limit and directly, which is accomplished in the first part of Sec. V together with the comparison with those earlier obtained results in the literature [28,29].

However, before proceeding to incorporation of the Kelvin effect in Sec. IV, another extension of the basic model will be tested in Sec. III. Namely, we shall explore a possible role of the kinetic resistance to phase change (defined by a Hertz-Knudsen-Schrage-like expression). Herewith, we shall have $\vartheta_{\rm mic} = \vartheta_{\rm mic}(\Sigma, K)$, where K is the kinetic resistance number to be defined in Sec. III, the basic model being recovered at $K = 0$. Later on, at the end of Sec. V, a similar study of the role of the kinetic resistance will be undertaken in application to the regime with an extended microfilm to disclose the dependency $\vartheta_{\rm mic} = \vartheta_{\rm mic}(K, {\rm Ke})$.

To recapitulate the organization of the present paper, the basic de Gennes-type model will be treated in Sec. II, which will be supplemented by the kinetic resistance to phase change in Sec. III. In Sec. IV, the basic model will rather be supplemented by the Kelvin effect and transitions from the truncated- to extended-microfilm regime will be studied. The regime with an extended microfilm will further be considered in Sec. V by direct means, which at the end of Sec. V will be supplemented by yet incorporating the kinetic resistance.

Then, in Sec. VI, we shall discuss the implications of the present study on the comparison with experimental results undertaken in Refs. [28,29]. At last, our conclusions will be summarized in Sec. VII. Certain mathematical details are relegated to appendices. Appendix A provides some coordinate expansions of the solution at the extremes of the domain that did not find their way into the main text of the paper. Appendix B serves as a supplement to Sec. V and revisits the asymptotic analysis of Ref. [28] in the limit of small Kelvin numbers with the aim to yet calculate a higher-order correction and thereby reconcile the asymptotic and present numerical results.

II. BASIC MODEL

The formulation of the basic model was provided in Ref. [12]. Here we take up its main points. The steady lubrication equation governing the liquid film profile $h^*(x^*)$ in the microregion can be

[2]In Refs. [28,29], a dimensionless number $\mathscr{L}$ is rather defined, a counterpart of the present Kelvin number as discussed in Sec. IV.

written in a standard way (e.g., Ref. [35] and, closer to the present context, Refs. [12,36]) as

$$q^{*\prime} + \frac{j^*}{\rho_l^*} = 0,\ q^* = -\frac{h^{*3}}{3\mu_l^*} p_l^{*\prime},\ p_l^* = p_0^* - \gamma^* h^{*\prime\prime} - \frac{\gamma^* a^{*2}}{h^{*3}}, \tag{5}$$

where q^* is the volume flux along the film, p_l^* is the pressure in the film determined by the Laplace and disjoining pressure contributions (p_0^* being a constant), the asterisk marks the dimensional quantities, while the prime denotes a derivative with respect to x^*. The evaporation flux j^* [kg/m^{2}s] is represented by the classical integrable divergence near the contact line of a thin film,

$$j^* = \frac{D_g^* \rho_{v,\mathrm{sat}}^*}{(\ell^* x^*)^{1/2}}, \tag{6}$$

where the tip of the film is chosen at $x^* = 0$, ℓ^* (considered known in the microregion analysis) is a macroscopic length scale given by Eq. (2) for a thin sessile droplet in a diffusion-limited regime of evaporation assuming for simplicity a zero ambient humidity (e.g., Refs. [37,38]). The boundary conditions at the tip of the film, starting abruptly at the solid surface, are

$$h^* \to 0, \quad \frac{1}{2}\gamma^* (h^{*\prime})^2 - \frac{\gamma^* a^{*2}}{2h^{*2}} \to -S^*,\ q^* \to 0 \quad \text{as } x^* \to 0. \tag{7}$$

The second condition is just the one of equilibrium at the tip of the film that needs to be formulated as such in a situation when the disjoining pressure law $\gamma^* a^{*2}/h^{*3}$ is formally assumed to hold down to $h^* = 0$ as it is here [11,12,31].[3] In view of the small scales of the microregion, the curvature therein is much greater than the macroscopic curvature. Therefore, at the outer (macroscopic) edge of the microregion, the curvature must fall to asymptotically smaller values than in the microregion, i.e., to zero at leading-order approximation. Thus,

$$h^* \to +\infty,\ h^{*\prime\prime} \to 0 \quad \text{as } x^* \to +\infty, \tag{8}$$

where h^* and x^* must tend to much greater values than in the microregion, i.e. formally to infinity at leading-order approximation. Thus, the basic model is formulated in the domain $0 < x^* < +\infty$ (the bare surface being located at $x^* < 0$). These conditions at infinity given by Eq. (8) actually boil down to a constant-slope behavior,

$$h^* \sim \theta_{\mathrm{mic}}\, x^* \quad \text{as } x^* \to +\infty. \tag{9}$$

The quantity θ_{mic} is unknown and must be found together with the solution of the problem. It is clearly the apparent contact angle as seen from larger scales, which in our context and for perfectly wetting liquids ($S^* > 0$) is just the evaporation-induced angle (cf. Sec. I). By using Eq. (8) or Eq. (9) in Eq. (5), we see that $p_l^* \to p_0^*$ and $p_l^{*\prime} \to 0$ as $x^* \to +\infty$ as expected, meaning that the pressure gradients fall to much smaller values than in the microregion towards the macroscopic domain. At the same time, as it follows from Eq. (6) and the first Eq. (5), the influx into the microregion from the macroscopic domain must go like $q^* = O(x^{*1/2})$ as $x^* \to +\infty$, not converging to any definite value, to compensate for the evaporation losses in our steady microregion at rest. This makes no contradiction with the second Eq. (5), where q^* is a product of a vanishing term, $p_l^{*\prime}$, and a diverging term, h^{*3}, which can resolve into the required behavior at infinity. Note that the liquid velocity associated with the influx decays then as $q^*/h^* = O(x^{*-1/2})$ as $x^* \to +\infty$ on account of Eq. (9).

This concludes the formulation of the basic model. We now proceed to nondimensionalization. For any dimensional quantity f^* (with asterisk), its dimensionless counterpart will be designated as

[3]However, in Ref. [12], we missed to explicitly mention the third of these conditions (expressing the absence of a line source at the tip of the film), although it was tacitly meant throughout.

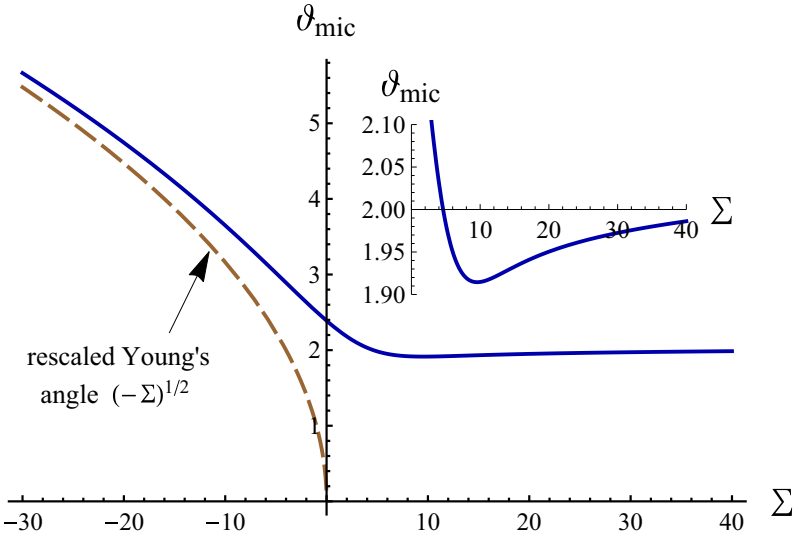

FIG. 2. Solid line: rescaled evaporation-induced contact angle $\vartheta_{\rm mic}$, which is actually the prefactor in a classical scaling law given by Eqs. (1)–(3) for the evaporation-induced contact angle, computed as a function of the dimensionless spreading coefficient Σ, Eq. (4), in the framework of the basic model. Dashed line: Young's angle in the same scaling for comparison (defined only for $\Sigma < 0$—partial wetting). Inset: details near the minimum of the curve.

f (without asterisk), whereas $[f]$ will denote the scale used. Thus,

$$f = f^*/[f]. \tag{10}$$

As already elaborated in Ref. [12], we use the scales

$$[x] = \frac{\sqrt{3}\,a^*}{\epsilon^2},\ [h] = \frac{\sqrt{3}\,a^*}{\epsilon},\ [j] = \frac{D_g^*\rho_{v,\rm sat}^*\epsilon}{3^{1/4}(\ell^* a^*)^{1/2}}, \tag{11}$$

where it is the choice of ϵ in the form of Eq. (1) that permits to scale the parameters out of the lubrication equation for $h(x)$ given by Eqs. (5). The latter equation then now reads

$$(h^3 h''' - h^{-1}h')' + j = 0, \tag{12}$$

with the dimensionless form of Eq. (6) given by

$$j = \frac{1}{\sqrt{x}}. \tag{13}$$

Equation (12) with (13) can be integrated once to yield

$$h^3 h''' - h^{-1}h' + 2\sqrt{x} = 0, \tag{14}$$

the integration constant vanishing in view of a zero volume flux as $x \to 0$. The dimensionless form of the boundary conditions given by Eqs. (7) and (8) reads

$$h \to 0,\ (h')^2 - \frac{1}{3h^2} \to -\Sigma \quad \text{as } x \to 0, \tag{15}$$

$$h \to +\infty,\ h'' \to 0 \quad \text{as } x \to +\infty, \tag{16}$$

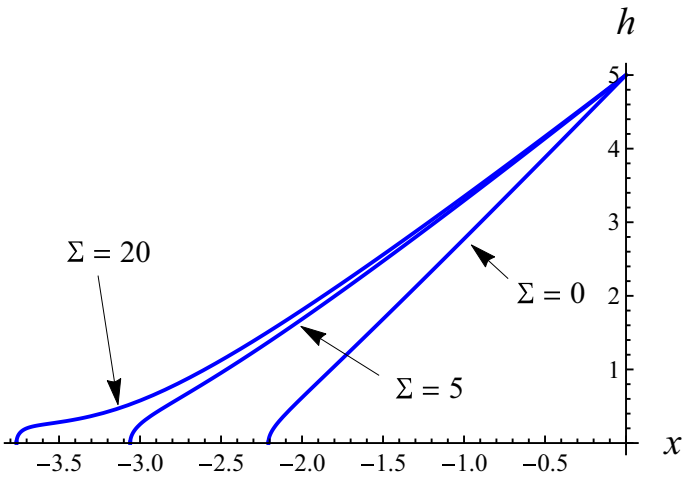

FIG. 3. Computed dimensionless microregion film profiles $h(x)$ at different values of the dimensionless spreading coefficient ($\Sigma = 0,\ 5$ and 20) in the framework of the basic model. For comparative purposes, each profile has been shifted so as to have $h = 5$ at $x = 0$. The scales are defined in Eq. (11).

where Σ is as in Eq. (4). Just as earlier with the dimensional versions given by Eqs. (8) and (9), Eq. (16) amounts to the behavior

$$h \sim \vartheta_{\mathrm{mic}}\, x \quad \text{as } x \to +\infty, \tag{17}$$

where ϑ_{mic} is the prefactor in Eq. (3), a rescaled apparent contact angle, to be determined together with the solution of the problem. Thus, the dimensionless formulation of the basic model is given by Eqs. (14)–(17). It depends on a single parameter Σ, hence $\vartheta_{\mathrm{mic}} = \vartheta_{\mathrm{mic}}(\Sigma)$ as foreseen in Sec. I based on the developments in Ref. [12].

The numerical solution of this third-order boundary-value problem can be obtained by shooting from $x \approx 0$ towards $x \gg 1$ aiming at $h'' = 0$. The point $x = 0$ presents a "benign" singularity, with the solution behaving as $h \sim (\frac{4}{3})^{1/4} x^{1/2}$ as $x \to 0$. This is a consequence of assuming a disjoining pressure of the form $\propto h^{-3}$ down to $h = 0$, and the intricacies thereof are discussed in Ref. [12]. Further developing the coordinate expansion, one obtains (cf. Eq. (39) in Ref. [12])

$$h \sim \left(\frac{4}{3}\right)^{1/4} x^{1/2}\left[1 - \frac{3^{1/2}}{4}\Sigma x - \frac{6}{5}x^{3/2}\ln x - \frac{2^{3/2}}{5\times 3^{3/4}}\Omega x^{3/2} - \frac{3}{32}\Sigma^2 x^2 + O(x^{5/2}\ln x)\right] \quad \text{as } x \to 0, \tag{18}$$

where Ω is a free coefficient which can be used in the shooting procedure.

Computation results for this problem were not provided in Ref. [12]. We rather show them here in Figs. 2 and 3. Figure 2 presents $\vartheta_{\mathrm{mic}}(\Sigma)$, which together with Eqs. (1), (3), and (4) yields the sought values of the evaporation-induced contact angle according to the basic de Gennes-type model. Although the primary focus in the present paper is on perfectly wetting liquids (i.e., $\Sigma \geqslant 0$), Fig. 2 also shows the extension of the result into the partial-wetting domain $\Sigma < 0$. In this latter domain, θ_{mic} is not an evaporation-induced contact angle in its entirety, but is rather an evaporation-modified Young's angle. The true Young's angle, in original terms $(2S^*/\gamma^*)^{1/2}$ (thin-film approximation) and $(-\Sigma)^{1/2}$ in terms of the rescaling given by Eq. (3), is also shown for comparison in Fig. 2 by the dashed line. In the perfect-wetting domain ($\Sigma \geqslant 0$), the dependence of ϑ_{mic} (and hence of the

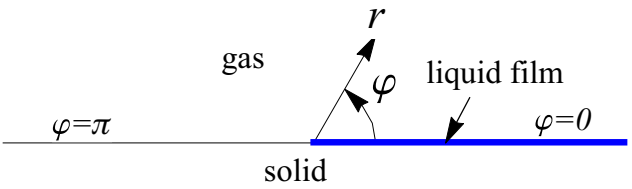

FIG. 4. Geometric sketch of the vapor diffusion problem in the gas. The liquid layer is of negligible thickness at the scale of the gas phase and corresponds to $\varphi = 0$ in terms of the polar coordinates $\{r, \varphi\}$ centered at the tip of the liquid layer ($\varphi = \pi$ at the bare solid surface).

evaporation-induced angle $\theta_{\rm mic}$) on the spreading coefficient Σ is seen to be remarkably weak and at the same time nonmonotonic.[4,5]

Figure 3 shows examples of the film profile in the microregion. One can appreciate the tendency for the film tip to become sharper and more protruding as Σ is increased (and hence as the film is made more wetting), which is rather intuitive. One can show that it is actually the de Gennes' pancake [12,30,32,33] that starts to protrude from the film profile, similar what was shown in the counterpart case of conduction-limited evaporation into pure vapor [12,36]. It is therefore for $\Sigma \gg 1$ that it becomes legitimate to use the pancake as the condition at the tip of film, cf. the approach in Refs. [24–26].

III. BASIC MODEL + KINETIC RESISTANCE TO EVAPORATION

The effect of kinetic resistance to evaporation consists in a deviation from local phase equilibrium under the conditions of sufficiently strong evaporation flux. This may be of especial relevance in the microregion, inherently associated with an evaporation flux singularity. The basic model (Sec. II) proceeded from the assumption of local phase equilibrium throughout, which ensured Eq. (6) and (13) along the entire microregion. In the present section, we explore how this can be modified due to the kinetic resistance and the possible consequences thereof upon the evaporation-induced contact angle.

To that purpose, we delve into the vapor concentration field, here described in terms of the partial vapor density ρ_v^*. Equation (6) corresponds in fact to a "corner" solution $\rho_v^* = \rho_{v,\rm sat}^* - 2\rho_{v,\rm sat}^*(r^*/\ell^*)^{1/2}\sin(\varphi/2)$, with the lowest possible positive power of r^*, of the steady diffusion (Laplace) equation $\nabla^{*2}\rho_v^* = 0$ satisfying a local phase equilibrium condition $\rho_v^* = \rho_{v,\rm sat}^*$ at the film $\varphi = 0$ and a zero-flux condition at the bare solid surface $\varphi = \pi$. Here $\{r^*, \varphi\}$ are the polar coordinates centered at the tip of the film, cf. Fig. 4. Furthermore, consistent with the thin-film approximation used in the present paper, the film thickness is neglected at the scale of the gas phase, so as for the film to approximately correspond to $\varphi \approx 0$ (Fig. 4). The diffusion-limited evaporation flux is then given by $j^* = -D_g^* r^{*-1}\partial\rho_v^*/\partial\varphi|_{\varphi=0}$, yielding indeed Eq. (6) for the mentioned corner solution.

[4]Interestingly, the dependencies $\vartheta_{\rm mic}(\Sigma)$ turns out to be quite similar in the present case of diffusion-limited evaporation into air and in the counterpart case of conduction-limited evaporation into pure vapor (cf. Fig. 5 in Ref. [12] for the latter). Note though that these are just the prefactors in Eq. (3), the expressions for ϵ being quite different between those two cases.

[5]One can show that the angle scale h_0/x_0 used in Refs. [24–26] is equal to $2^{1/3}\epsilon$ in present terms. The value of the prefactor can be read from their figure 2 (static case) and is approximately equal to 1.42. In our present terms, this corresponds to $\vartheta_{\rm mic} \approx 1.42 \times 2^{1/3} \approx 1.8$, which is slightly below the typical values of $\vartheta_{\rm mic}$ encountered in Fig. 2 in the case of perfect wetting.

Now, once the kinetic resistance is incorporated into the model, the condition $\rho_v^* = \rho_{v,\mathrm{sat}}^*$ is replaced at $\varphi = 0$ by

$$\rho_v^* - \rho_{v,\mathrm{sat}}^* = -\frac{2 - f_a}{2 f_a}\left(\frac{2\pi M^*}{R_g^* T^*}\right)^{1/2} j^* \tag{19}$$

in accordance with the Hertz-Knudsen-Schrage equation (see, e.g., Ref. [39] and references therein; an ideal-gas relation $\rho_v^* = p_v^* M^*/(R_g^* T^*)$ was used as necessary, where p_v^* is the partial vapor pressure). Here f_a is what is sometimes referred to as the accommodation coefficient, and sometimes the evaporation/condensation coefficient. Ideally, $f_a = 1$. In reality, $0 < f_a < 1$ and its values can in principle vary very significantly [39]. With this modification, the mentioned corner solution and Eq. (6) are no longer valid throughout. However, they must still hold asymptotically as x^*, $r^* \to +\infty$, when Eq. (19) reduces back to the phase equilibrium consistently with $j^* \to 0$ according to Eq. (6). In other words, a new solution for $\rho_v^*(r^*, \varphi)$ and $j^*(x^*)$ must tend to them at infinity.

It will be more convenient to work in terms of the deviation from the vapor density at saturation

$$\tilde{\rho}_v^* = \rho_v^* - \rho_{v,\mathrm{sat}}^*. \tag{20}$$

In addition to Eq. (11), we shall use the scales

$$[r] = [x] = \frac{\sqrt{3}\, a^*}{\epsilon^2}, \quad [\tilde{\rho}_v] = \rho_{v,\mathrm{sat}}^* \left(\frac{[x]}{\ell^*}\right)^{1/2}. \tag{21}$$

Note in passing that as ℓ^* is a macroscopic length, e.g., Eq. (2), whereas $[x]$ a microscopic one (the longitudinal extent of the microregion), we actually have $[x] \ll \ell^*$, and hence $[\tilde{\rho}_v] \ll \rho_{v,\mathrm{sat}}^*$. The formulated problem for the vapor concentration can then be written in dimensionless terms as

$$\frac{\partial^2 \tilde{\rho}_v}{\partial r^2} + \frac{1}{r}\frac{\partial \tilde{\rho}_v}{\partial r} + \frac{1}{r^2}\frac{\partial^2 \tilde{\rho}_v}{\partial \varphi^2} = 0, \tag{22}$$

$$\tilde{\rho}_v \sim -2 r^{1/2} \sin\frac{\varphi}{2} \quad \text{as } r \to +\infty, \tag{23}$$

$$\partial \tilde{\rho}_v / \partial \varphi = 0 \quad \text{at } \varphi = \pi, \tag{24}$$

$$j = -\frac{1}{r}\frac{\partial \tilde{\rho}_v}{\partial \varphi} \quad \text{at } \varphi = 0, \tag{25}$$

$$\tilde{\rho}_v = -K\, j \quad \text{at } \varphi = 0, \tag{26}$$

where note that $r \equiv x$ at $\varphi = 0$. Here

$$K = \frac{l_K^*}{[x]} = \frac{l_K^* \epsilon^2}{\sqrt{3}\, a^*}, \quad l_K^* = D_g^* \frac{2 - f_a}{2 f_a}\left(\frac{2\pi M^*}{R_g^* T^*}\right)^{1/2} \tag{27}$$

are the kinetic-resistance number and length, respectively. Note that the basic model (Sec. II) is recovered therefrom as $K \to 0$.

For an estimation of typical values, we take $D_g^* \sim 10^{-5}\,\mathrm{m}^2/\mathrm{s}$, $f_a = 1$ (ideal case), $M^* \sim 50\,\mathrm{g/mol}$, $R_g^* = 8.31\,\mathrm{J/mol\,K}$, and $T^* \sim 300\,\mathrm{K}$. One then obtains $l_K^* \sim 50\,\mathrm{nm}$. However, for $a^* \sim 0.3\,\mathrm{nm}$ and taking into account that according to Eq. (3) and Fig. 2 we have roughly $\epsilon \sim \theta_{\mathrm{mic}}/2$ (θ_{mic} in radians), one obtains $[x] \sim 270\,\mathrm{nm}$ for $\theta_{\mathrm{mic}} \sim 5^\circ$ and $[x] \sim 70\,\mathrm{nm}$ for $\theta_{\mathrm{mic}} \sim 10^\circ$. This corresponds to $K \sim 0.2$ for $\theta_{\mathrm{mic}} \sim 5^\circ$ and $K \sim 0.8$ for $\theta_{\mathrm{mic}} \sim 10^\circ$, which seem to be quite moderate values. Note though that for $f_a < 1$ (nonideal case, which is quite probable [39]), much higher values of K can in principle ensue.

The solution of the problem given by Eqs. (22)–(26) is obtained numerically, of which we are most interested in $j(x)$. Note that it actually suffices to solve the problem only once, say, for $K = 1$, yielding $j(x)$ that we shall for the moment denote $j_1(x)$. Then, at any K, the evaporation flux profile

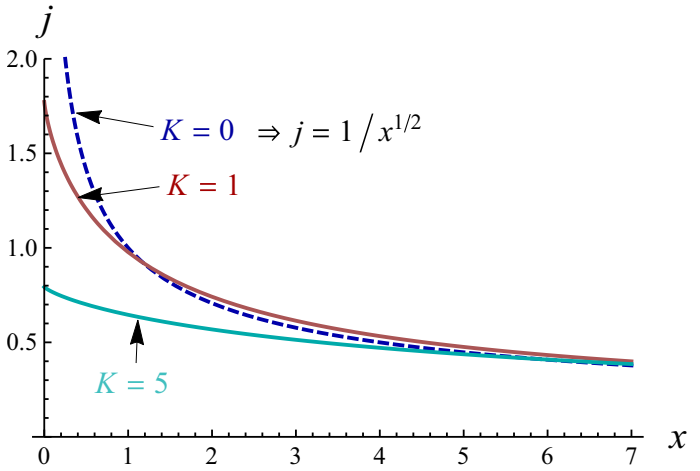

FIG. 5. Solid lines: computed dimensionless evaporation flux distribution $j(x)$ along the microregion for a finite kinetic resistance to evaporation ($K = 1$ and $K = 5$) in the framework of the basic model + kinetic resistance. Dashed line: the same distribution in the absence of kinetic resistance ($K = 0$), implying a local thermodynamic equilibrium throughout, as given by Eq. (13) and used in the basic model. The scales are defined in Eq. (11) while the parameter K in Eq. (27). At any K, we have $j(x) = K^{-1/2} j_1(x/K)$, where $j_1 \equiv j$ at $K = 1$ shown in the plot.

will be given by $j(x) = K^{-1/2} j_1(x/K)$, which can be established by a simple rescaling in Eqs. (22)–(26). Figure 5 shows the profiles $j(x)$ at $K = 1$ and $K = 5$, and for comparison their counterpart at $K = 0$ given by Eq. (13). We see that, at a finite kinetic resistance, the evaporation flux remains finite at the tip of the film $x = 0$, unlike what we have in the absence of the kinetic resistance. The profiles asymptotically merge towards large x, of course.

We are now ready for the final step: solving the problem for the film profile. The formulation remains essentially the same as for the basic model in Sec. II, except that the evaporation flux must no longer be used in the form of Eq. (13). It is now rather the newly calculated K-dependent profiles $j(x)$ that must be injected into Eq. (12). Accordingly, instead of Eq. (14), the integrated form of the equation now becomes

$$h^3 h''' - h^{-1} h' + J = 0, \quad J = \int_0^x j(\check{x})\, d\check{x},$$

where $J(x)$, an integral evaporation flux, is a beforehand known function for each K (the film and the evaporation problems are decoupled). The boundary conditions remain as in Eqs. (15)–(17). The problem is solved in the same way as in Sec. II, by means of the shooting method.

Results for $\vartheta_{\rm mic}(\Sigma, K)$ in the perfectly wetting domain ($\Sigma \geqslant 0$) are presented in Fig. 6, where note that the curve of Fig. 2 is recovered at $K = 0$. We see that the evaporation-induced angle decreases as K is increased, which is what should be expected given that the kinetic resistance mitigates the evaporative singularity (cf. Fig. 5). However, the dependence on K, just as the dependence on Σ, turns out to be relatively weak, the most sharp variation of $\vartheta_{\rm mic}$ occurring at smaller values of Σ and K. Remarkably, a nonmonotonic behavior of $\vartheta_{\rm mic}$ versus Σ is seen to survive at finite kinetic resistances.

IV. BASIC MODEL + KELVIN EFFECT: TRANSITION FROM TRUNCATED TO EXTENDED ADSORBED MICROFILMS

In the basic model, the saturation density and pressure of the vapor are just constants. However, given the small size of the microregion, and hence large values of the curvature, Laplace and

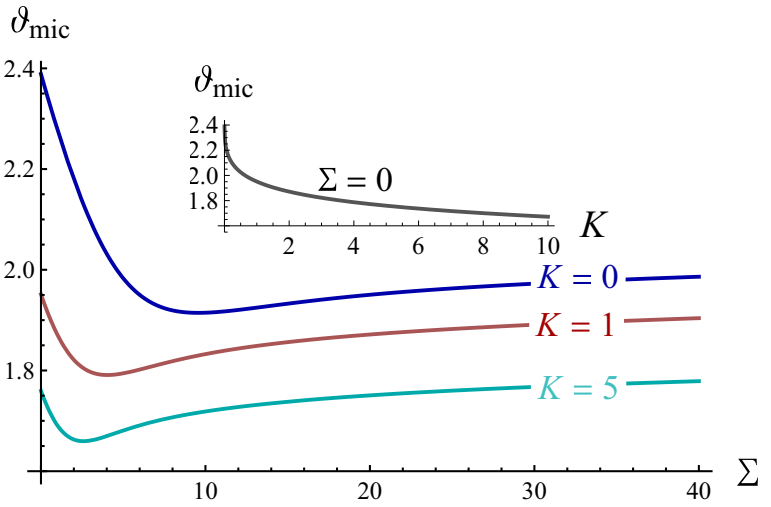

FIG. 6. The same as in Fig. 2, but now in the framework of the basic model + kinetic resistance for a few values of the kinetic resistance number $K = 0,\ 1,$ and 5. Inset: ϑ_{mic} versus K for $\Sigma = 0$. The result for $K = 0$ exactly coincides with the one of Fig. 2.

disjoining pressures, there may occur essential deviations of these saturation quantities from their usual values, what is known as the Kelvin effect. To have an appreciable influence on what is going on in the microregion, such deviations need not even be comparable to the original values; the saturation-density deviation $\Delta\rho^*_{v,\mathrm{sat}}$ just needs to attain the order of magnitude of $[\tilde{\rho}_v]$ in Eq. (21), which was shown in Sec. III to be much smaller than $\rho^*_{v,\mathrm{sat}}$ itself. Thermodynamics relates $\Delta\rho^*_{v,\mathrm{sat}}$ to the difference between the liquid and vapor pressures, which in the present situation is principally given by the sum of the Laplace and disjoining pressures:

$$\Delta\rho^*_{v,\mathrm{sat}} = -\rho^*_{v,\mathrm{sat}}\frac{M^*\gamma^*}{\rho^*_l R^*_g T^*}\left(h^{*\prime\prime} + \frac{a^{*2}}{h^{*3}}\right). \tag{28}$$

This is a linearized version of a more general relation, valid for $\Delta\rho^*_{v,\mathrm{sat}} \ll \rho^*_{v,\mathrm{sat}}$ and sufficient in the present context in line with the above reasoning.

In the present section, we once again disregard the kinetic resistance to evaporation, whose consideration stays bound to Sec. III. In exchange, we now supplement the basic model with the Kelvin effect and study the consequences thereof. As the saturation density, now $\rho^*_{v,\mathrm{sat}} + \Delta\rho^*_{v,\mathrm{sat}}$, will vary along the microregion in accordance with Eq. (28), we shall need, as in Sec. III, a detailed consideration of vapor diffusion in the gas phase adjacent to the microregion, rather than merely resorting to Eq. (6) or (13). At the same time, once again as in Sec. III, the evaporation-flux expressions given by Eqs. (6) and (13) will still be relevant, but now just as asymptotic behaviors at the outer edge of the microregion, as $x \to +\infty$, when $\Delta\rho^*_{v,\mathrm{sat}} \to 0$ together with $h^{*-1} \to 0$ and $h^{*\prime\prime} \to 0$, cf. Eqs. (8) and (28).

Furthermore, the formulation of the vapor diffusion problem developed in Sec. III is actually *verbatim* applicable to the present situation with the only, yet paramount exception of the boundary condition at the liquid film. Namely, instead of Eq. (19) at $\varphi = 0$, we now have

$$\rho^*_v = \rho^*_{v,\mathrm{sat}} + \Delta\rho^*_{v,\mathrm{sat}}. \tag{29}$$

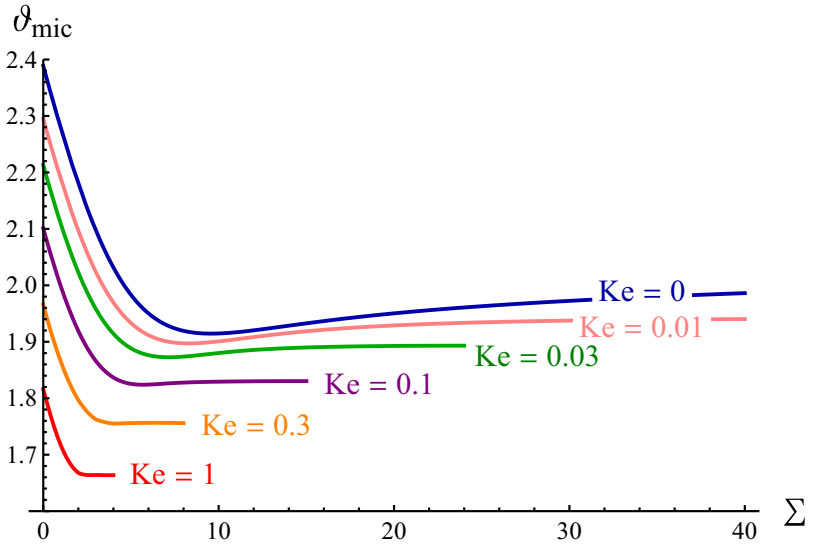

FIG. 7. The same as in Fig. 2, but now in the framework of the basic model + Kelvin effect for a number of values of the Kelvin number Ke = 0, 0.01, 0.03, 0.1, 0.3 and 1. Ke is defined in Eq. (31) and related as $\mathscr{L} = 3 \times 2^{4/9}\mathrm{Ke}^{4/3}$ to the Laplace parameter $\mathscr{L}$ used in Refs. [28,29]. The result for Ke = 0 exactly coincides with the one of Fig. 2.

Likewise, in the dimensionless terms still introduced by means of Eqs. (11) and (21), the boundary condition given by Eq. (26) is now replaced with

$$\tilde{\rho}_v = -\mathrm{Ke}\left(3h'' + \frac{1}{h^3}\right) \quad \text{at } \varphi = 0, \tag{30}$$

following from Eqs. (20), (28), and (29). Here

$$\mathrm{Ke} = \frac{\delta^{*2}\epsilon}{3a^{*2}}, \quad \delta^* = \left(\frac{\rho^*_{v,\mathrm{sat}}\nu^*_l D^*_g M^*}{\rho^*_l R^*_g T^*}\right)^{1/2} \tag{31}$$

are the Kelvin number[6] and length, respectively (the counterpart of δ^* in the pure-vapor case was introduced in Refs. [16,20]). Note that the basic model (Sec. II) is recovered in the limit Ke $\to$ 0.

For an estimation of typical values, we take up the material property values used when estimating ϵ and K in Secs. I and III as well as $\rho^*_l \sim 1000\,\mathrm{kg/m^3}$. We obtain $\delta^* \sim 0.2\,\mathrm{nm}$, Ke ~ 0.01. Obviously, larger values of δ^* and Ke can occur for more volatile liquids, with larger $\rho^*_{v,\mathrm{sat}}$. For instance, we obtain Ke ~ 0.05 for pentane.[7]

To recapitulate, the dimensionless formulation of the basic model + Kelvin effect is given by Eqs. (12), (15), (16) [or rather Eq. (17)], (22)–(25), and (30). The two parameters of the problem, Σ and Ke, are defined in Eqs. (4) and (31), respectively. The scales and renormalizations used are still given by Eqs. (1)–(3), (11), and (21).

In spite of the above used similarity with the problem considered in Sec. III (basic model + kinetic resistance), the present problem (basic model + Kelvin effect) is actually more complex

[6]The Laplace parameter $\mathscr{L}$ introduced in Ref. [28], cf. also Ref. [29], is hereby expressed as $\mathscr{L} = 3 \times 2^{4/9}\mathrm{Ke}^{4/3}$.

[7]From an estimation $\mathscr{L} \sim 0.08$ given in Ref. [29] and using a conversion between $\mathscr{L}$ and Ke provided in an earlier footnote 6.

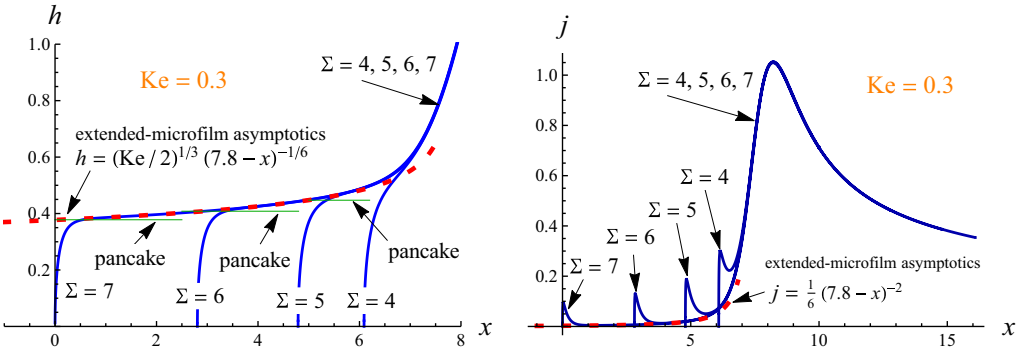

FIG. 8. Solid lines: computed dimensionless microregion film profiles $h(x)$ (left) and evaporation flux profiles $j(x)$ (right) within the basic model + Kelvin effect at Ke = 0.3 for a number of values $\Sigma = 4,\ 5,\ 6$ and 7. Dashed lines: extended-microfilm asymptotics. All profiles except for $\Sigma = 7$ are suitably x-shifted so as to highlight their actual partial overlapping. Horizontal thin solid lines (left) indicate the pancake thickness $\Sigma^{-1/2}$ for some film profiles. The scales are defined in (11). For comparison, the film profiles shown in Fig. 3 correspond to Ke = 0 in current terms.

from the mathematical viewpoint. Indeed, in the former problem, we could first obtain once and for all the vapor concentration field $\tilde{\rho}_v$ and the evaporation flux distribution j, and then merely use them (namely, j) in the film part of the formulation to calculate h. In other words, the vapor part of the problem was decoupled from the film part. This is no longer so with the Kelvin effect: the condition given by Eq. (30) shows that the two are now coupled and must be resolved simultaneously. Thus, the shooting method used in Secs. II and III is no longer applicable. Instead, we used a discretization of the equations and boundary conditions by means of second-order finite differences (including the Laplace Eq. (22) in a two-dimensional domain $\{r, \varphi\}$ typically using 1500×250 points). A strongly graded grid was used, with a higher resolution near the tip of the film, by making a variable change like $r = \ln \xi$ and using a uniform grid in terms of ξ. To treat the boundary conditions at the singular points $x, r \to 0$ and $x, r \to \infty$, the corresponding coordinate expansions were developed (see Appendix A), so that the actual boundary conditions were replaced by patching the numerical solution to the coordinate expansions at some sufficiently small and large values of x and r. Such use of the coordinate expansions in particular allowed to achieve a high degree of independence of the numerical domain size for quite moderate values thereof (the maximum values of x and r typically used being of the order of 50, and their minimum values of the order of 10^{-4}). The resulting system of nonlinear algebraic equations for the values of $\tilde{\rho}_v$, j and h at the grid points and free coefficients of the coordinate expansions such as ϑ_{mic} in Eq. (17) or Ω in Eq. (18) was resolved by means of the `FindRoot` command in *Mathematica*.

The results for $\vartheta_{\text{mic}}(\Sigma, \text{Ke})$ are shown in Fig. 7. Apart from a decrease with an increase of the Kelvin number, a most remarkable feature is that ϑ_{mic} appears to attain a constant at sufficiently large dimensionless spreading coefficients Σ. The latter is seen to occur for each finite value of Ke, whereas in the absence of the Kelvin effect (Ke = 0) ϑ_{mic} appears to grow indefinitely with Σ.

The physical reasons for such behavior become clear in Fig. 8, representing film profiles (left) and evaporation-flux profiles (right) at different Σ. The profiles corresponding to $\Sigma = 4,\ 5,$ and 6 are shifted along x so as for all profiles to largely overlap along their main parts, to the right of the truncated microfilms. What is truly essential here is that they *can* be made to practically overlap in this way. At the same time, the length of the truncated microfilm is seen to rapidly grow with Σ, which is not unexpected given that larger Σ correspond to a more wetting situation. In fact, we already saw signs of such growth in Fig. 3 in the framework of just the basic model (without the Kelvin effect), although the presence of the Kelvin effect makes it appreciably more drastic (Fig. 8 left). Indeed, the Kelvin effect is seen to significantly regularize the evaporation-flux

profiles (Fig. 8 right), no longer diverging as Eq. (13) at the tip of the film (and now tending to Eq. (13) only at $x \gg 1$), hence letting the truncated microfilms extend more without vaporizing. Incidentally, this evaporation singularity reduction also goes along with lowering the ϑ_{mic} values already pointed out for Fig. 7. Again, what seems to be truly essential in Fig. 8 is that the growing (with Σ, but at the same Ke) truncated microfilms follow a "channel" specified by the dashed curve in Fig. 8 (left), which is nothing else than the *extended* adsorbed microfilm profile $h = (\mathrm{Ke}/2)^{1/3}(-x)^{-1/6}$ [cf. Eq. (34) and Sec. V in what follows], suitably shifted along x. Thus, we see that, at sufficiently large Σ, we practically attain the extended-microfilm regime within the family of truncated-microfilm ones, the truncated microfilm deemed to formally extend to infinity as $\Sigma \to +\infty$. At the same time, the evaporation-flux profile associated with the extended adsorbed microfilm is $j = \frac{1}{6}x^{-2}$ [cf. Eq. (39) and Sec. V in what follows], which is indeed attained within the family of truncated-microfilm regimes as Σ is increased (Fig. 8 right; once again implying a shift along x). Note also a small local burst of the flux that remains near the tip of the truncated microfilm.

Coming back to Fig. 7, the reason for the curves to reach constant values at large Σ is now clear: these values of ϑ_{mic} must already practically correspond to the extended-microfilm regime, independent of Σ. To verify the point, we carried out our computation directly for the extended-microfilm regime (see the next section, Sec. V, for more details). The results for ϑ_{mic} proved to be within less than 1% from those obtained for the truncated-microfilm regime at sufficiently large Σ, thus demonstrating the point.

One can note that the transition from the truncated- to the extended-microfilm regime of the microregion occurs in the present case of diffusion-limited evaporation into air in a somewhat different way than in the case of conduction-limited evaporation into pure vapor studied in Ref. [11]. Here, it occurs asymptotically in the limit $\Sigma \gg 1$. There, it occurs at a finite critical value of Σ, above which the truncated-microfilm regime ceases to exist at all. This difference can be traced back to the fact that, here, the extended microfilm thickness decays away from the main part of the microregion, cf. Fig. 8 (left), whereas, there, its thickness remains constant. Indeed, the earlier mentioned de Gennes' pancake has a dimensionless thickness $\Sigma^{-1/2}$ [12], decreasing with Σ. Therefore, here, the pancake thickness can actually never fall below the extended microfilm thickness whatever large Σ could be: there will always be a location corresponding to the pancake thickness along the decaying extended microfilm. This will roughly be the location of the truncated-microfilm tip (cf. Fig. 8 left), hence an asymptotic estimation $\ell_{\mathrm{mf}} \sim \frac{1}{4}\mathrm{Ke}^2\Sigma^3$ for the dimensionless length of the truncated microfilm in the limit $\Sigma \gg 1$, the scale being $[\ell_{\mathrm{mf}}] = [x]$, cf. Eq. (11). In contrast, there, the pancake thickness simply falls below the extended-microfilm thickness above a certain critical value of Σ, signifying the end of the truncated-microfilm regime in favor of the extended-microfilm one [11]. The present situation is in this sense closer not to its above-mentioned pure-vapor counterpart, but rather to the microregion of an advancing contact line of a perfectly wetting nonvolatile liquid studied in Ref. [31]. The present extended-microfilm regime appears to be a full counterpart of the "maximal" solution by Hervet and de Gennes [31] (cf. also Ref. [12]), to which the truncated-microfilm solutions tend in the limit of large spreading coefficients.

Let us also note the following. The extended-microfilm regime formally exists (is a solution) irrespective of the value of the spreading coefficient, since it involves no actual three-phase contact. However, in accordance with thermodynamic and kink-propagation arguments put forth in Ref. [11], an adsorbed microfilm is metastable (with respect to the bare substrate state) when its thickness is smaller than the pancake thickness. In the present context, with an asymptotically decaying extended-microfilm thickness falling below the pancake thickness above a certain distance, this indicates that it is the truncated-microfilm regime that is actually realized for any finite Σ, the extended-microfilm regime being just a valuable limiting case corresponding to $\Sigma \gg 1$.

V. FURTHER RESULTS FOR THE REGIME WITH AN EXTENDED ADSORBED MICROFILM

The consideration in Sec. IV led us, among other things, to results for the (more classical) regime with an extended adsorbed microfilm, which were obtained both as a limit $\Sigma \gg 1$ within the

family of the regimes with a truncated microfilm and, for verification, by means of a computation directly proceeding from the extended-microfilm formulation. It is worthwhile to dwell more upon the extended-microfilm problem, which we accomplish in the present section. This is all the more so given that, to the best of our knowledge, no exact, numerical solution of the problem in question was previously reported in the literature (meaning the case of a diffusion-limited evaporation into air). Indeed, the previous pioneering works by Eggers and Pismen [23], by Doumenc and Guerrier [27], and by Morris [28] either relied upon an asymptotic approach [28], or considered a global problem and not explicitly a microregion one [23,27].

Needless to recall that the consideration is still carried out in the framework of the scales and renormalizations given by Eqs. (1)–(3), (10), (11), (21). Practically all equations and boundary conditions used for the basic model + Kelvin effect in Sec. IV remain of the same form here, except for the geometric domain of their applicability: the liquid layer now occupies the whole solid substrate surface $-\infty < x < +\infty$, and not just $x \geqslant 0$ as before. The sole boundary condition that also implies a change of the form is an asymptotic condition for the extended adsorbed microfilm as $x \to -\infty$ (see below) now replacing Eq. (15) at the truncated-microfilm tip. Besides, Eq. (24) is now lost since no bare substrate surface is available anymore. For the same reason, Σ is no longer explicitly present among the parameters of the problem (Ke remaining the only one). The new geometry makes it more convenient to proceed in terms of the Cartesian coordinates $\{x, z\}$ in lieu of the earlier used polar coordinates $\{r, \varphi\}$ ($x = r\cos\varphi$, $z = r\sin\varphi$). Here z is the one orthogonal to the substrate surface, $z = 0$ corresponding to the surface itself, and the scale being just $[z] = [x]$. Thus, the mathematical formulation for the regime with an extended adsorbed microfilm can be recapitulated as

$$h^3 h''' - h^{-1} h' + J = 0, \quad J = \int_{-\infty}^{x} j(\check{x})\, d\check{x}, \tag{32}$$

$$h' = \vartheta_{\mathrm{mic}} \quad \text{as } x \to +\infty, \tag{33}$$

$$h \sim \left(\frac{\mathrm{Ke}}{2}\right)^{1/3} (-x)^{-1/6} \quad \text{as } x \to -\infty, \tag{34}$$

$$\frac{\partial^2 \tilde{\rho}_v}{\partial x^2} + \frac{\partial^2 \tilde{\rho}_v}{\partial z^2} = 0 \qquad (z > 0), \tag{35}$$

$$\tilde{\rho}_v \sim -2r^{1/2} \sin \tfrac{1}{2}\varphi \quad \text{as } r \to +\infty \tag{36}$$

$$\text{with} \quad r = (x^2 + z^2)^{1/2}, \quad \varphi = \arccos \frac{x}{(x^2 + z^2)^{1/2}},$$

$$j = -\frac{\partial \tilde{\rho}_v}{\partial z} \quad \text{at } z = 0, \tag{37}$$

$$\tilde{\rho}_v = -\mathrm{Ke}\left(3h'' + \frac{1}{h^3}\right) \quad \text{at } z = 0. \tag{38}$$

The asymptotic behavior given by Eq. (34), corresponding to the extended adsorbed microfilm, is deduced from Eq. (38) on account of Eq. (36), the latter giving rise to $\tilde{\rho}_v|_{z=0} \sim -2(-x)^{1/2}$ as $x \to -\infty$. Using Eq. (34) in the film Eq. (32), one can deduce

$$j \sim \frac{1}{6x^2} \quad \text{as } x \to -\infty. \tag{39}$$

Both Eqs. (34) and (39) were already referred to without derivation in Sec. IV and, with an x-shift, in Fig. 8.

Consider now the coordinate expansion of the solution for the concentration field at infinity [recall that some other coordinate expansions throughout the paper are relegated to Appendix A, cf., e.g., Eq. (A1) for h as $x \to +\infty$, unless of immediate use for the discussion as the present one].

One arrives at

$$\tilde{\rho}_v \sim -2r^{1/2}\sin\frac{\varphi}{2} + C_1 r^{-1/2}\sin\frac{\varphi}{2} - (6r)^{-1}\sin\varphi + o(r^{-1}) \quad \text{as } r \to +\infty. \tag{40}$$

Equation (40) contains a few higher-order terms in addition to the leading-order behavior represented in Eq. (36). These are solutions of Eq. (35) with two boundary conditions: (i) Eq. (37) on account of Eq. (39), and (ii) $\tilde{\rho}_v|_{z=0} = o(x^{-1})$ as $x \to +\infty$, the latter following from Eqs. (33) and (38). The second term on the right-hand side is a "corner solution" of the same type as the first term, C_1 being a free coefficient. The third term is engendered by the mass transfer in the extended absorbed microfilm Eq. (39). One can easily verify that, given an asymptotic nature of the expression, the second term merely amounts to an x-shift within the first term. The problem given by Eqs. (32)–(38) is actually invariant with respect to shifts along x, the asymptotic boundary conditions at infinity representing just the leading-order behaviors. Thus, without loss of generality, one can merely choose $C_1 = 0$, which amounts to fixing the reference point along the x axis and which is what is implied in what follows. The behavior given by Eq. (40) can be used to deduce the asymptotic behaviors of the local and integral evaporation fluxes, j and $J = \int_{-\infty}^{x} j(\check{x})\,d\check{x}$, as $x \to +\infty$ (which will be useful in what follows). For j, this is straightforward by using Eq. (37). In the case of J, for any positive x, one can write

$$J = \int_{-\infty}^{-x} j(\check{x})\,d\check{x} + \int_{-x}^{x} j(\check{x})\,d\check{x} = \int_{-\infty}^{-x} j(\check{x})\,d\check{x} + \int_0^{\pi} \left(-\frac{\partial\tilde{\rho}_v}{\partial r}\Big|_{r=x}\right) x\,d\varphi,$$

where the second term was transformed in to an integral over a half-circle of radius $r = x$ on account of the integral form of species conservation in the diffusion problem. Now assuming $x \gg 1$ and using Eqs. (39) and (40), we obtain the final result. Thus,

$$j \sim \frac{1}{x^{1/2}} + \frac{1}{6x^2}, \quad J \sim 2x^{1/2} - \frac{1}{6x} \quad \text{as } x \to +\infty, \tag{41}$$

where we chose $C_1 = 0$ in accordance with the earlier made convention.

The numerical approach adopted here is essentially the same as the one described in Sec. IV, except that the problem was now treated and discretized in the Cartesian coordinates in a large rectangular domain $\{-x_{\max} \leqslant x \leqslant x_{\max}, 0 \leqslant z \leqslant z_{\max}\}$, where $x_{\max}$ and $z_{\max}$ are large positive values (we typically used $x_{\max} = z_{\max} \sim 40$). The patching to the coordinate expansions was now realized at the three sides of the rectangle remote from the origin. A change of the independent variables, viz. $x = \sinh\xi$ and $z = \sinh\eta$, was applied so as to discretize at a uniform grid in terms of ξ and η (typically using 1000×500 points) and render the grid more dense in terms of x and z near the origin. Computations using various domain sizes and numbers of grid points (e.g., both varied by a factor of two in both directions from the typical values) were carried out so as to verify that the results did not change within a certain precision (<0.1% for the ϑ_{mic} values reported here).

Figure 9 displays the here computed dependence of $\vartheta_{\text{mic}}(\text{Ke})$ in the extended-microfilm regime (solid line). It is notably a decreasing function of Ke, in accordance with what was already observed in Fig. 7. A number of asymptotic results for $\vartheta_{\text{mic}}(\text{Ke})$ pertaining to the limits of either small Ke (dashed lines) or large Ke (dot-dashed line) are also shown for comparison.

Among these asymptotic results in Fig. 9 is most notably the one derived in Ref. [28] (cf. also Ref. [29]) in the limit $\text{Ke} \ll 1$ (short-dashed line).[8] While the trend is certainly well captured, one

[8] We use the representation given in Ref. [29], cf. Eqs. (3.6) and (3.7) therein, of the asymptotic result obtained in Ref. [28]. Comparing these to Eqs. (1)–(3), we arrive at

$$\vartheta_{\text{mic}} = \left(\frac{3^{1/4}}{(\pi^2/2)^{1/6}}\right)^{-1} k \approx 0.99\,k \quad \text{with} \quad k = 1.47758\,\frac{2^{1/6}}{\pi^{1/3}}\,W\!\left(\frac{4}{\mathscr{L}^{3/2}}\right)^{1/6},$$

where W is the Lambert W function (the inverse of $W\exp W$), while a relation between $\mathscr{L}$ and Ke is given in an earlier footnote 6.

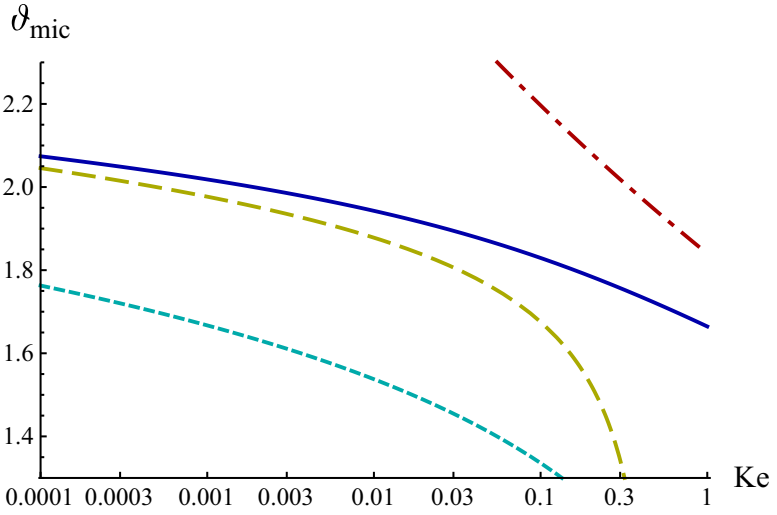

FIG. 9. Rescaled evaporation-induced contact angle ϑ_{mic}, the prefactor in a classical scaling law given by Eqs. (1)–(3) for the evaporation-induced contact angle, *versus* the Kelvin number Ke in the microregion regime with an extended adsorbed microfilm (no kinetic resistance yet considered, $K = 0$). Solid line: our present computation. Short-dashed line: asymptotic result in the limit $\mathrm{Ke} \ll 1$ obtained in Ref. [28] and also used in Ref. [29]. Long-dashed line: ditto but now also including a higher-order correction obtained in Appendix B. Dot-dashed line: asymptotic result in the limit $\mathrm{Ke} \gg 1$ adapted from Ref. [40].

nonetheless observes a nonnegligible underprediction of the numerical ϑ_{mic} values persisting even at rather small values of Ke (the short-dashed curve lying noticeably lower than the solid one in Fig. 9). An earlier indication that such an underprediction could occur can in fact be found in Ref. [29], based on a test computation in the framework of the global sessile-drop model from Ref. [23].[9] The existence of such a discrepancy is actually not overly unexpected given a logarithmic character of the asymptotic expansion here, the smallness parameter being essentially $(\ln \mathrm{Ke})^{-1}$ rather than Ke itself. To clear up this point, we extended the asymptotic analysis of Ref. [28] to include the next logarithmic order in the asymptotic expansion (see Appendix B). The outcome is shown in Fig. 9 (long-dashed line). One can appreciate that the discrepancy is thereby drastically reduced, which confirms that a logarithmic correction can be rather appreciable even for Ke as low as $\mathrm{Ke} = 0.0001$ and serves to reconcile the numerical and asymptotic approaches.

At the same time, the asymptotic analyses confirm what one could suspect on the basis that the very existence of an extended microfilm here depends on the Kelvin effect. Namely, they confirm that the problem is singular and no finite limit is attained by ϑ_{mic} as $\mathrm{Ke} \to 0$ in the regime with an extended microfilm. Rather, ϑ_{mic} must continue to grow indefinitely, even if very slowly (logarithmically). This is quite in contrast with the regime with a truncated microfilm, for which the problem can be considered at $\mathrm{Ke} = 0$ exactly (viz. the basic model, Sec. II, does not include the Kelvin effect) and for which ϑ_{mic} attains finite values as $\mathrm{Ke} \to 0$ (cf., e.g., Fig. 7).

[9]Indeed, the latter yielded a prefactor value $k = 1.9$ ($\vartheta_{\mathrm{mic}} \approx 1.88$), a higher value than $k = 1.69$ ($\vartheta_{\mathrm{mic}} \approx 1.67$) resulting from Ref. [28] under the same conditions. Here recall that $\vartheta_{\mathrm{mic}} \approx 0.99\,k$ (cf. an earlier footnote). However, $k = 1.9$ is still somewhat lower than $k \approx 2.04$ ($\vartheta_{\mathrm{mic}} \approx 2.02$) that we would obtain here (cf. the solid line of Fig. 9). This is not too surprising given that the test computation actually concerned a small drop near extinction ($R_c^* = 10^3 a^*$, i.e., $R_c^* \sim 0.5\,\mu\mathrm{m}$ for typically $a^* \sim 0.5\,\mathrm{nm}$), so that a large negative "macroscopic" curvature and a fast (accelerating towards extinction) receding of the contact line would result in a reduction of the apparent contact angle.

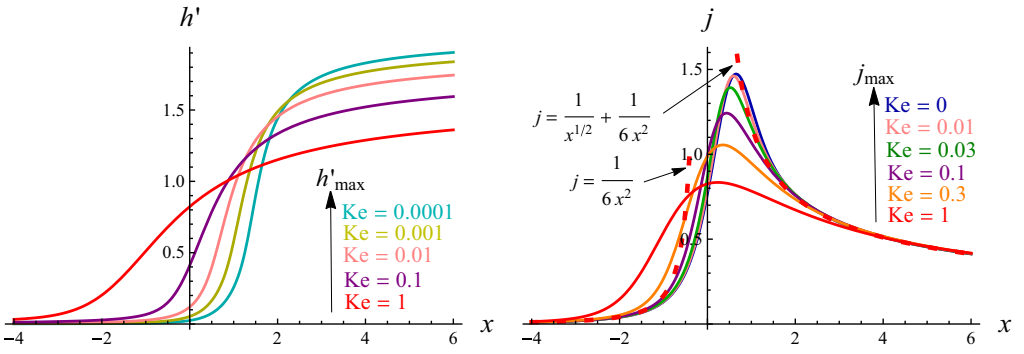

FIG. 10. Computed dimensionless microregion profiles (solid lines) of the film slope $h'(x)$ for Ke = 0.0001, 0.001, 0.01, 0.1, and 1 (left) and evaporation flux $j(x)$ for Ke = 0, 0.03, 0.1, 0.3, and 1 (right). Regime with an extended adsorbed microfilm (and no kinetic resistance, $K = 0$). The scales are defined in Eq. (11). The maximum values of both h' and j decrease with increasing Ke, which permits to establish an unambiguous correspondence between a given profile and its Ke value. Asymptotic behaviors given by Eqs. (39) and (41) (dashed lines).

Also displayed in Fig. 9 (dot-dashed line) is what can be considered as an asymptotic result in the limit of large Ke. It is based on the developments of Ref. [40], where the disjoining pressure is completely disregarded while the Kelvin effect (due to the Laplace pressure) remains the only regularizing mechanism in the microregion (cf. Ref. [36] for the counterpart of the large-Ke limit in the pure-vapor case).[10]

The film-slope and evaporation-flux profiles computed for the regime with an extended microfilm are represented in Fig. 10 for various Ke. One can see that the evaporation-flux profiles $j(x)$ become sharper (viz. higher and narrower) as Ke is decreased. Furthermore, they are seen to attain a finite limiting form as Ke $\to 0$, in spite of the overall problem with an extended microfilm being singular as Ke $\to 0$ as already mentioned. This is in fact fully in line with the predictions of the asymptotic analysis of Ref. [28], where a corresponding reduced problem was formulated permitting to compute $j(x)$ at Ke $= 0$ exactly. This is precisely how it was computed here for Fig. 10 (right), see Appendix B for further details. Another related feature evidenced by Fig. 10 is that the maximum of the h' growth shifts more and more to the right as Ke $\to 0$ while the position of the maximum evaporation rate remains fixed. In other words, the zone where an essential part of the evaporation-induced contact angle is formed gets separated from the maximum evaporation rate, the latter progressively finding itself in the zone of the adsorbed microfilm. This also agrees with the asymptotic picture developed in Ref. [28] in the limit Ke $\to 0$. At the same time, Fig. 10 provides a hint at the possible physical nature of the earlier discussed underprediction of $\vartheta_{\rm mic}$ by means of the asymptotic theory [28]: the evaporation flux j to the right of the zone of h' maximum growth still appears to remain quite nonnegligible, even if well smaller than at the j maximum, which can still contribute to the buildup of the final slope $\vartheta_{\rm mic} = h'|_{x\to+\infty}$ (see Appendix B for more details).

Thus far, the basic model has been supplemented by either the kinetic resistance (Sec. III) or the Kelvin effect (Sec. IV and the present section up to now) separately. We now consider their joint action, but limit ourselves to the regime with an extended adsorbed microfilm under study in the present section. The condition given by Eq. (38) is then replaced with

$$\tilde{\rho}_v = -\mathrm{Ke}\left(3h'' + \frac{1}{h^3}\right) - K\,j \quad \text{at } z = 0 \tag{42}$$

[10]Comparing Eqs. (1)–(3) here to Eqs. (4.2) and (4.6) in Ref. [40], the latter can be rendered as $\vartheta_{\rm mic} = 1.84\,\mathrm{Ke}^{-1/13}$ in our present terms, which is the dot-dashed curve plotted in Fig. 9.

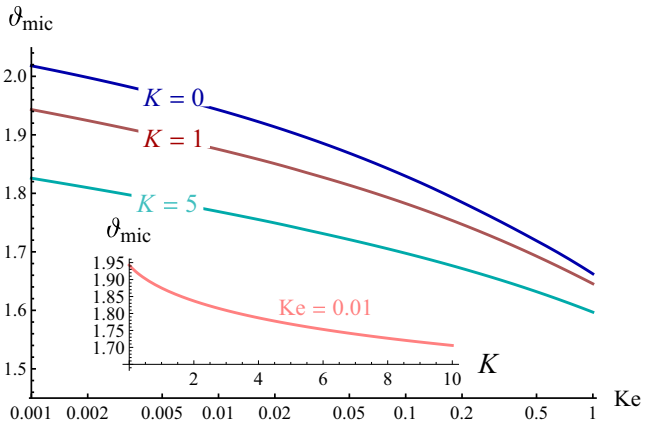

FIG. 11. Dependence on the kinetic resistance in the extended-microfilm regime. The result for $K = 0$ (no kinetic resistance) reproduces the solid curve of Fig. 9, and its counterparts for $K = 1$ and 5 are also represented. Inset: ϑ_{mic} versus K at $\mathrm{Ke} = 0.01$.

[in essence, we end up with a combination of terms present in Eq. (26), on the one hand, and in Eq. (30) or Eq. (38), on the other hand]. The formulation remains unchanged otherwise. We shall hereby study how the kinetic resistance affects the evaporation-induced angles for the extended-microfilm regime. This is reduced to a dependence on two parameters: $\vartheta_{\mathrm{mic}} = \vartheta_{\mathrm{mic}}(K, \mathrm{Ke})$, among which Σ does not appear since the extended-microfilm regime does not depend on the spreading coefficient [unlike a truncated-microfilm regime, where one would have a dependence $\vartheta_{\mathrm{mic}} = \vartheta_{\mathrm{mic}}(\Sigma, K, \mathrm{Ke})$]. The computation results are provided in Fig. 11. We observe quite a modest influence of the kinetic resistance, which is even somewhat weaker (with no drastic change at small K) than what we already saw in Fig. 6 in the framework of the basic model. The latter fact is not surprising given that the kinetic resistance gives rise to a regularization of the evaporation flux singularity in the framework of the basic model (cf. the two curves in Fig. 5), whereas it merely exerts a smooth effect in the case of an extended adsorbed microfilm *a priori* involving no such singularities.

VI. IMPLICATIONS FOR COMPARISON WITH EXPERIMENT

A detailed comparison of the predicted evaporation-induced contact angles with the experimental results reported in Refs. [22,41,42] was undertaken in Ref. [28]. The measured values were thereby found to fall below the predicted ones roughly at a ratio of 0.9 for octane, 0.8 for HMDS and 0.7 for nonane and OMTS (for sessile drops with a radius $R_c^* \sim 1$ mm). However, as already mentioned in Sec. V, although our present formulation for the regime with an extended adsorbed microfilm (at $K = 0$) is exactly the same (up to notations) as the one originally put forth and used in Ref. [28], it was an asymptotic method that Ref. [28] proceeded from, whereas an exact, numerical solution is used in the present paper. In accordance with the discrepancy between the solid and short-dashed curves of Fig. 9, this implies that, in reality, the agreement with the experiments turns out to be less good than reported in Ref. [28], the earlier mentioned ratios needing to be modified by a factor[11]

[11]Between the various experiments processed in Ref. [28], the parameter $\mathscr{L}$ was found to vary between 0.00046 and 0.041 [28]. In terms of Ke (cf. an earlier footnote 6 for the relation between $\mathscr{L}$ and Ke), this implies a variation between $\mathrm{Ke} = 0.0011$ and $\mathrm{Ke} = 0.032$. Accordingly, the ratio of the ϑ_{mic} values at the short-dashed and solid curves of Fig. 9 is found to vary between 0.83 and 0.77. To simplify, we just use 0.8 throughout.

$\sim$0.8 and hence becoming roughly 0.7 for octane, 0.65 for HMDS and 0.55 for nonane and OMTS. The reason for such a discrepancy is not clear without further study.

Likewise, given that Ref. [29] also relied upon the asymptotic result of Ref. [28] for comparison to their own measurements, a similar "numerical rectification" as above can be applied to their study too. To judge by their figure 6, this rectification will lead to an even greater overprediction of their measured contact angle values than what they already had for nonane, octane and heptane. On the contrary, for more volatile liquids with larger evaporation-induced contact angles (hexane and pentane), the rectification will improve the agreement with experiment to a good level. Further study of this issue is required, in particular to investigate whether an essential thermal-Marangoni inflation of the drop revealed in Ref. [43] for more volatile liquids distorts the contact-angle measurements.

Let us now see whether accounting for the other physical effects studied in the present paper, such as the possibility of the adsorbed microfilm getting truncated and the kinetic resistance to evaporation, can substantially reduce the above-mentioned discrepancy with experiment. In other words, we shall see whether one can end up with substantially lower values of ϑ_{mic} thanks to those two effects. A certain improvement towards this goal appears to be possible for sufficiently small Ke in the realm of truncated microfilms as manifest in Fig. 7 by the minima of the curves occurring at a finite value of Σ. However, a maximum reduction of ϑ_{mic} achievable in this way is just from $\vartheta_{\mathrm{mic}} \sim 2.0$ (cf. the solid curve of Fig. 9 at small Ke) to $\vartheta_{\mathrm{mic}} \sim 1.9$ (cf. the inset of Fig. 2), i.e., no more than $\sim$5%, which is too small to substantially correct the discrepancy with experiment. For the kinetic resistance, our earlier estimations yielded at most $K \sim 1$, hence (cf. the results for $K = 0$ and $K = 1$ in Fig. 11) once again a maximum reduction of $\sim$5%. It is only anomalously low values of the accommodation coefficient in Eq. (27), e.g., as found for water in Ref. [39], that could in principle lead to much larger values of K and make a difference here. However, this does not seems to be an *a priori* viable possibility. Thus, we conclude that the two considered effects are not sufficient to take care of the discrepancy.

VII. CONCLUDING REMARKS

We have extended an approach due to de Gennes and collaborators to the problem of evaporation-induced apparent contact angles of perfectly wetting liquids undergoing diffusion-limited evaporation into air. As a main usable output of the analysis, the prefactor ϑ_{mic} entering a classical scaling law for such angles, cf. Eqs. (1)–(3), has been calculated in various formulations, in the order of increasing mathematical and physical complexity. Finer details of the liquid-film profiles in the microregion have also been analyzed.

We started from a simplest possible formulation ("basic model"), where the mechanical action of the disjoining pressure, in the form of an inverse cubic law, alone enables the singularity resolution in the microregion where such angles are established. The evaporation-induced contact angle has been found to be only slightly dependent, by means of the prefactor, on the spreading coefficient in the perfectly wetting case. Interestingly though, this dependence turned out to be nonmonotonic. The microregion film profiles are, in this formulation, abruptly starting off a bare solid surface. At larger values of the spreading coefficient, a truncated microfilm (assimilated to a precursor film) starts to develop from the overall microregion film profile, resembling more distinctly a protruding de Gennes' pancake.

The inclusion of the kinetic resistance to evaporation eliminates the evaporation-flux divergence at the contact line and leads to somewhat smaller values of the evaporation-induced contact angle. The biggest rate of such angle reduction has been found to occur at smaller spreading coefficients and at smaller values of the kinetic resistance.

The inclusion of the Kelvin effect has similarly been found to lead to a quite moderate reduction of the angles. A most important structural Kelvin-related change consisted in a pronounced elongation of the truncated microfilms for sufficiently large spreading coefficients, ultimately leading to the regime with an extended absorbed microfilm previously known in the literature [23,27,28]. Our computation for this extended-microfilm regime has yielded prefactor values somewhat greater

(by ∼20%) than known from earlier asymptotic approaches [28,29], a discrepancy that we have here successfully explained by accounting for a correction beyond the leading-order approximation within the asymptotic approach. However, this would imply a corresponding increase in the evaporation-induced angle estimations provided for numerous liquids in Refs. [28,29], which in most cases (for liquids less volatile than pentane) would somewhat worsen the agreement with experiment as compared to what was claimed in Refs. [28,29]. A parametric study within the present models (including the truncated-microfilm regimes and reasonable values of the kinetic resistance) revealed only a possible partial improvement as far as the agreement with experiment is concerned, indicating that the phenomenon may still depend on some other factor(s) not yet included into the models.

Finally, let us mention that the scenario of the transition from the truncated- to the extended-microfilm regime here turned out to closely resemble the one of Hervet and de Gennes [12,31], but to be somehow different from the pure-vapor counterpart [11] of the present study, in that the transition occurs asymptotically at large spreading coefficient values but not at a finite critical value thereof.

ACKNOWLEDGMENTS

The authors are grateful for the support from BELSPO PRODEX and European Space Agency MAP projects, and from the BELSPO IAP-7/38 MicroMAST project. P.C. gratefully acknowledges support from Fonds de la Recherche Scientifique–FNRS.

APPENDIX A: COORDINATE EXPANSIONS

Here we provide some relevant coordinate expansions of the solution of the problem at the extremes of the domain that did not already appear in the main text of the paper.

First, we turn to the basic model + Kelvin effect (Sec. IV). At the tip of the truncated microfilm, similarly to Eq. (18), one can deduce in a step-by-step way

$$h \sim \left(\frac{4}{3}\right)^{1/4} x^{1/2}\left[1 - \frac{3^{1/2}}{4}\Sigma x - \frac{2^{3/2}}{5\times 3^{3/4}}\Omega x^{3/2} - \frac{3}{32}\Sigma^2 x^2 - \frac{2\sqrt{2}(5c_1 + 3\sqrt{3}\,\mathrm{Ke}\,\Sigma\Omega)}{105\times 3^{3/4}\mathrm{Ke}} x^{5/2} + O(x^3)\right] \quad \text{as } x \to 0,$$

$$\tilde{\rho}_v \sim \mathrm{Ke}\,\Omega + c_1 r\cos\varphi - \frac{2\sqrt{2}c_1}{3^{7/4}\mathrm{Ke}} r^{3/2}\sin\frac{3\varphi}{2} + c_2 r^2\cos 2\varphi + O(x^{5/2}) \quad \text{as } r \to 0,$$

where Ω, c_1, and c_2 are free coefficients to be determined with the full solution. A noteworthy result from these expansions concerns $j = -x^{-1}\partial\tilde{\rho}_v/\partial\varphi|_{\varphi=0}$, cf. Eq. (25). We thereby obtain a behavior $j \sim \frac{\sqrt{2}c_1}{3^{3/4}\mathrm{Ke}} x^{1/2}$ as $x \to 0$, i.e. a local evaporation flux vanishing at the tip of the film (cf. Fig. 8 right), quite in contrast with a divergence given by Eq. (13) in the absence of the Kelvin effect. At infinity, supplementing the leading-order behavior given by Eq. (23) with a few higher-order terms, one arrives at

$$\tilde{\rho}_v \sim -2r^{1/2}\sin\frac{\varphi}{2} + C_1 r^{-1/2}\sin\frac{\varphi}{2} + O(r^{-3/2}\ln r) \quad \text{as } r \to +\infty,$$

where C_1 is a free coefficient. This is a solution of the Laplace Eq. (22) with the boundary conditions given by Eq. (24) and $\tilde{\rho}_v = 0$ at $\varphi = 0$. The latter is here actually Eq. (30) approximated up to the order considered on account of Eq. (17) yielding $\tilde{\rho}_v|_{\varphi=0} = o(r^{-1})$ as $r \to +\infty$ [more precisely, $\tilde{\rho}_v|_{\varphi=0} = O(r^{-3/2})$ on account of Eq. (A1) below]. As compared to Eq. (40), the term $O(r^{-1})$ is here absent, due to the absence of the extended microfilm but the presence of a bare substrate at $\varphi = \pi$ instead. Also in contrast with Eq. (40), C_1 cannot be set equal to zero but must rather be

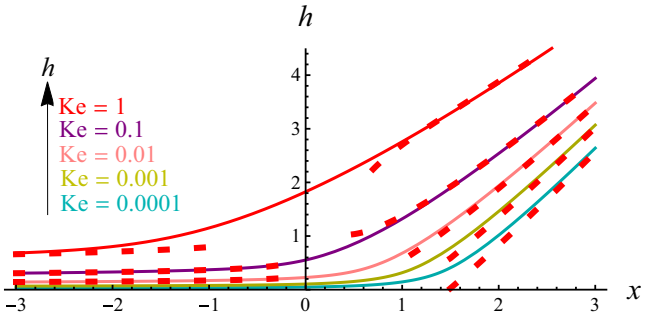

FIG. 12. Solid lines: computed dimensionless microregion film profiles $h(x)$ exactly corresponding to the slope profiles of Fig. 10 (left). Larger Ke correspond to larger h within the region shown. Dashed lines: for each case, the asymptotic behaviors given by Eq. (34) valid at large negative x (indiscernible and not shown for smaller Ke) and Eq. (A1) valid at large positive x with the free coefficients computed from the full solution. Here Eq. (A1) has been extended up to and including the order $O(x^{-1})$.

determined together with the full solution of the problem (the reference point along the x axis being here represented by the tip of the film located at $x = 0$ by definition).

Second, we also provide a generalization of Eq. (40) (extended-microfilm regime) in the case when the kinetic resistance is included ($K \neq 0$) as at the end of Sec. V:

$$\tilde{p}_v \sim -2r^{1/2}\sin\frac{\varphi}{2} - K\pi^{-1}r^{-1/2}\left(\ln r\sin\frac{\varphi}{2} + (\pi-\varphi)\cos\frac{\varphi}{2}\right)$$
$$+ C_1 r^{-1/2}\sin\frac{\varphi}{2} - (6r)^{-1}\sin\varphi + o(r^{-1}) \quad \text{as } r \to +\infty.$$

We note that the second (new) term on the right-hand side is a solution of the Laplace equation with the following boundary conditions: (i) $\partial\tilde{p}_v/\partial\varphi = 0$ at $\varphi = \pi$, which is a consequence of $j = r^{-1}\partial\tilde{p}_v/\partial\varphi|_{\varphi=\pi}$ from Eq. (39) actually decaying faster than $O(r^{-3/2})$ as $x \to -\infty$ ($r \to +\infty$, $\varphi = \pi$, $x = -r$) in the extended adsorbed microfilm, and (ii) $\tilde{p}_v = -Kr^{-1/2}$ at $\varphi = 0$ ($x = r$), which follows from Eq. (42) to leading order as $r \to +\infty$ upon the substitution of $j \sim x^{-1/2}$ [cf. Eq. (41)] and $h \sim \vartheta_{\text{mic}}x$.

Third, for all the models treated in the present paper, it turns out to be $j \sim x^{-1/2} + o(1)$ as $x \to +\infty$ while the liquid film is always governed by Eqs. (12) and (17) [note that Eqs. (32) and (33) are equivalent to those]. Then, deducing further terms of the coordinate expansion beyond Eq. (17) from Eq. (32), one can obtain

$$h \sim \vartheta_{\text{mic}}x - \frac{16}{3\vartheta_{\text{mic}}^3}x^{1/2} + B_1\ln x + B_0 + O(x^{-1/2}\ln x) \quad \text{as } x \to +\infty, \tag{A1}$$

where ϑ_{mic}, B_1, and B_0 are free coefficients to be determined with the full solution. Note though that the higher-order terms not displayed in Eq. (A1) generally adopt a model-dependent form, unlike the terms displayed. As illustrated in Fig. 12 for the liquid film profiles, the asymptotic behaviors expected at large positive and negative x manifest a high degree of overlapping with the full solution already at quite moderately large values of $|x|$.

APPENDIX B: REVISITING THE ASYMPTOTIC ANALYSIS AT SMALL Ke FOR THE REGIME WITH AN EXTENDED MICROFILM AND NO KINETIC RESISTANCE

This Appendix is motivated by the necessity to rationalize the noticeable discrepancy between the asymptotic results (the limit $\text{Ke} \ll 1$) of Ref. [28] and the present numerical results as it appears in Fig. 9. The foundations of the asymptotic approach and the leading-order approximation were

considered in great detail in Ref. [28]. Here the asymptotic analysis is reproduced in a concise formal way in our notations with a view to advancing one step further to a logarithmic correction beyond the leading order, with the help of which we shall seek to explain the discrepancy.

The asymptotic analysis of Ref. [28] reveals the existence of an "inner" ("tapered film") region where the Laplace pressure is negligible and a maximum evaporation rate j is attained, and, to its right, a relatively narrow "corner" region where a maximum growth of the film slope h' takes place. Such distinct spatial separation between the maximums of j and h' was noted to be compatible with the numerical solution of the full problem in Sec. V (cf. the discussion of the h' and j profiles at small values of Ke in Fig. 10). The slope growth in the corner region is a dynamic effect of a liquid flow passing through it to the inner region to compensate for the evaporative losses in the latter. However, the evaporation in the corner region itself and its dynamic influence are effects beyond the leading-order approximation.

Here we shall have to introduce yet another, "outer" region, to the right of the corner region. The outer region is trivial and needs not be distinguished in the framework of the leading-order approximation Ref. [28] was bound to. However, as we shall see, it *is* required when dealing with a higher-order correction, for the evaporation flux at larger x (behaving as $j = 1/x^{1/2}$ and $J = 2x^{1/2}$ there) still slightly contributes to building up the film slope so as to affect the final value $\vartheta_{\mathrm{mic}} = h'|_{x\to+\infty}$. Thus, we here eventually end up with three regions (inner, corner, and outer). Solutions are sought separately in each of them and joined by means of a matching procedure (matched asymptotic expansions).

1. Inner region

In the inner region, associated with the extended adsorbed microfilm, we have $h = O(\mathrm{Ke}^{1/3})$ as indicated by Eq. (34). Accordingly, we introduce a new dependent variable

$$\bar{h} = \mathrm{Ke}^{-1/3} h, \tag{B1}$$

so as to have $\bar{h} = O(1)$ there, whereas the independent variable x is not changed. Equation (34) can then be rewritten as

$$\bar{h} \sim (-4x)^{-1/6} \quad \text{as } x \to -\infty. \tag{B2}$$

The Laplace pressure contributions in Eqs. (32) and (38) are negligible to the leading order in $\mathrm{Ke} \ll 1$ in the inner region, and hence these equations rather become

$$-\bar{h}^{-1}\bar{h}' + J = 0, \quad J = \int_{-\infty}^{x} j(\check{x})\, d\check{x}, \tag{B3}$$

$$\tilde{\rho}_v = -1/\bar{h}^3 \quad \text{at } z = 0. \tag{B4}$$

Other equations and boundary conditions of the full problem with an extended microfilm, viz. Eqs. (35)–(37), remain formally unchanged within the leading order in the inner region except for Eq. (33), which is now incompatible with the film Eq. (B3) and must be replaced with another behavior at infinity. Assuming a sufficiently fast growth of $\bar{h}$ and hence [cf. Eq.(B4)] a sufficiently fast decay to zero of $\tilde{\rho}_v|_{z=0}$ as $x \to +\infty$ [verified *a posteriori* in Eq. (B5)], the behaviors given by Eqs. (40) and (41) still hold in the framework of the leading-order problem in the inner region. Using Eqs. (41) in (B3) and integrating, one obtains[12]

$$\bar{h} \sim c\, x^{-1/6} \exp\left(\tfrac{4}{3}x^{3/2}\right) \quad \text{as } x \to +\infty, \tag{B5}$$

[12]This is similar to Eq. (5.8) in Ref. [28]. Note that the different prefactors (4/3 here and 2/3 there) in front of $x^{3/2}$ are merely a consequence of the different scales used in the nondimensionalization and do not amount to a real discrepancy. However, the flux J correction $-\frac{1}{6}x^{-1}$ was not accounted for in Ref. [28], which would subsequently lead to missing a prefactor $x^{-1/6}$ in their equation as compared to Eq. (B5) here.

where c is a constant to be determined together with the full solution in the inner region. The fact that this solution fails to satisfy Eq. (33) and rather behaves as Eq. (B5) underscores once again the necessity of introducing yet another (corner) region, where the Laplace pressure would no longer be negligible and the behavior could be rectified toward Eq. (33).

To sum up, the leading-order problem in the inner region is given by Eqs. (35)–(37), (B2)–(B5). It does not depend on Ke. Up to notations, it is equivalent to the corresponding problem originally formulated in Ref. [28][13]

It turns out (cf. Ref. [28] and the next subsection) that to proceed to a leading-order consideration in the corner region one does not even need to know to value of c in Eq. (B5) or to otherwise know the inner-region solution other than just the exponential growth in the asymptotic condition given by Eq. (B5). However, on the one hand, we shall here be also interested in a (logarithmic) correction beyond the leading-order approximation, as it was already stated. On the other hand, the numerical code here developed for the full problem can straightforwardly be adapted for the problem in the inner region anyway. Thus, the computation yields $c = 0.80$. Another result of this computation is the evaporation-flux profile $j(x)$, represented in Fig. 10 (right) as corresponding to $\mathrm{Ke} = 0$ (exactly).

2. Corner region and the leading-order asymptotic result for ϑ_{mic}

In the corner region, new variables (with a hat) are introduced similarly to Ref. [28]:

$$x = \ell_1 + \Delta x\, \hat{x}, \quad h = \Delta h\, \hat{h}, \tag{B6}$$

where ℓ_1 (position of the corner region) is expected to be asymptotically large as $\mathrm{Ke} \to 0$, while the scales Δx and Δh asymptotically small (the corner region being narrow), which is confirmed in what follows. The Laplace pressure d^2h/dx^2 must no longer be negligible. For it to rather be comparable with the disjoining pressure $1/h^3$, the following scale choice is appropriate:

$$\Delta h = \Delta x^{1/2}. \tag{B7}$$

Matching between the inner and corner regions is to be accomplished by means of the asymptotic behavior given by Eq. (B5). Rewriting the latter in terms of the corner variables on account of Eqs. (B1), (B6), and (B7), and carrying out some series expansions on account of the supposed asymptotic order of the parameters, one obtains

$$\hat{h} \sim \mathrm{Ke}^{1/3} \Delta h^{-1} c\, \ell_1^{-1/6} \left(1 - \frac{\Delta x\, \hat{x}}{6\, \ell_1}\right) \exp\left(\frac{4}{3}\ell_1^{3/2} + 2\ell_1^{1/2} \Delta x\, \hat{x} + \frac{(\Delta x\, \hat{x})^2}{2\, \ell_1^{1/2}}\right). \tag{B8}$$

Since both $\hat{x}$ and $\hat{h}$ are defined so as to be $O(1)$ in the corner region, the scales can be chosen such that

$$\mathrm{Ke}^{1/3} \Delta h^{-1} c\, \ell_1^{-1/6} \exp\left(\tfrac{4}{3}\ell_1^{3/2}\right) = 1, \quad 2\ell_1^{1/2} \Delta x = 1. \tag{B9}$$

The parameters ℓ_1, Δx and Δh are now fully determined by the system of Eqs. (B7) and (B9), from where one can see that ℓ_1 is logarithmically large, while Δx and Δh are logarithmically small as $\mathrm{Ke} \to 0$ (thus confirming the original expectations concerning their largeness or smallness). Their following combinations will hereafter be of special relevance:

$$\zeta \equiv \frac{\Delta x}{\ell_1} = 12\left[W\left(\frac{3\mathrm{Ke}^{-6}}{64\, c^{18}}\right)\right]^{-1}, \quad \hat{\epsilon} \equiv \frac{\Delta h}{\Delta x} = \left(\frac{4}{\zeta}\right)^{1/6}, \tag{B10}$$

where W is the Lambert W function (the inverse of $W \exp W$, as already mentioned), $\hat{\epsilon}$ is the film slope scale in the corner region (logarithmically large), and ζ is the small parameter defining the first logarithmic correction to the leading-order approximation. The latter fact becomes evident as

[13] See Eq. (5.3) therein.

soon as Eq. (B8) gets rewritten, on account of Eqs. (B7), (B9), and (B10) and an additional series expansion within the exponential term, as

$$\hat{h} \sim \left[1 + \tfrac{1}{4}\zeta\left(\hat{x}^2 - \tfrac{2}{3}\hat{x}\right)\right] \exp \hat{x}. \tag{B11}$$

We note that the terms of an order higher than the first logarithmic correction are neglected in Eq. (B11) and in what follows. Estimation of ζ at $\mathrm{Ke} = 0.001$ and $\mathrm{Ke} = 0.0001$ (recalling that $c = 0.8$) yields $\zeta = 0.31$ and $\zeta = 0.23$, respectively. These are quite nonnegligible values so that a possible explanation of the discrepancy motivating this Appendix by means of a logarithmic correction indeed appears to be a viable path.

We note that in the corner region (and later on in the outer region) the dimensionless vapor concentration deviation $\tilde{\rho}_v$ at the film surface turns out to be algebraically small in Ke, cf. Eq. (38), whereas we are here dealing with logarithmic corrections at most. Therefore, in these regions, we essentially have $\tilde{\rho}_v = 0$ so that the evaporation flux is merely given by $J = 2x^{1/2} - \frac{1}{6}x^{-1}$ in accordance with Eq. (41) with no need to reconsider the diffusion problem in the gas phase. Using this expression and Eq. (B6) with Eq. (B7) and Eq. (B10) in Eq. (32) and expanding in $\zeta \ll 1$ up to and including $O(\zeta)$, one obtains the following film equation in the corner region:

$$\hat{h}^3 \frac{d^3\hat{h}}{d\hat{x}^3} - \hat{h}^{-1}\frac{d\hat{h}}{d\hat{x}} + 1 + \zeta\left(\frac{1}{2}\hat{x} - \frac{1}{6}\right) = 0.$$

The solution is sought by perturbations:

$$\hat{h} = \hat{h}_0 + \zeta\, \hat{h}_1, \tag{B12}$$

so that $\hat{h}_0$ and $\hat{h}_1$ satisfy the equations

$$\hat{h}_0^3 \frac{d^3\hat{h}_0}{d\hat{x}^3} - \hat{h}_0^{-1}\frac{d\hat{h}_0}{d\hat{x}} + 1 = 0, \tag{B13}$$

$$\hat{h}_0^3 \frac{d^3\hat{h}_1}{d\hat{x}^3} + 3\,\hat{h}_0^2\hat{h}_1 \frac{d^3\hat{h}_0}{d\hat{x}^3} - \hat{h}_0^{-1}\frac{d\hat{h}_1}{d\hat{x}} + \hat{h}_0^{-2}\hat{h}_1\frac{d\hat{h}_0}{d\hat{x}} + \frac{1}{2}\hat{x} - \frac{1}{6} = 0. \tag{B14}$$

At large negative $\hat{x}$, the solution must match the one from the inner region, i.e., the form of Eq. (B11), hence the boundary conditions

$$\hat{h}_0 \sim \exp \hat{x}, \quad \hat{h}_1 \sim \tfrac{1}{4}\left(\hat{x}^2 - \tfrac{2}{3}\hat{x}\right) \exp \hat{x} \quad \text{as } \hat{x} \to -\infty.$$

At large positive $\hat{x}$ we seek to satisfy Eq. (17), i.e., $\hat{h} \to +\infty$, $d^2\hat{h}/d\hat{x}^2 \to 0$ as $\hat{x} \to +\infty$ in terms of the variables with a hat. One can then deduce the following asymptotic behaviors:

$$\hat{h}_0 \sim \hat{b}_0\hat{x} - \frac{1}{2\hat{b}_0^3}\ln\hat{x} + \ldots, \quad \hat{h}_1 \sim \frac{1}{2\hat{b}_0^3}\hat{x}\ln\hat{x} + \hat{b}_1\hat{x} + \ldots \quad \text{as } \hat{x} \to +\infty, \tag{B15}$$

where note a logarithmic divergence of the slope at infinity for the correction. Here $\hat{b}_0$ and $\hat{b}_1$ are constants to be determined together with the solution of the boundary-value problem for $\hat{h}_0$ and $\hat{h}_1$. In fact, for $\hat{h}_0$, it was already solved in Refs. [28,36] yielding in particular[14] $\hat{b}_0 = 1.123$. Likewise, resolving the boundary-value problem for $\hat{h}_1$, one obtains $\hat{b}_1 = -0.578$.

We are now in a position to represent the leading-order result for ϑ_{mic} in the limit $\mathrm{Ke} \ll 1$. Indeed, $\vartheta_{\mathrm{mic}} = dh/dx|_{x\to+\infty} \approx \hat{\epsilon}\, d\hat{h}_0/d\hat{x}|_{\hat{x}\to+\infty} = \hat{b}_0\hat{\epsilon}$ to leading order. On account of Eq. (B10),

[14]Equation (5.22a) of Ref. [28] contains a different prefactor as compared to our counterpart given by Eq. (B13). Therefore, to obtain ours from their result given by Eq. (6.1) one should yet divide the latter by $3^{1/4}$: $1.47758/3^{1/4} \approx 1.123$.

one obtains

$$\vartheta_{\mathrm{mic}} = \hat{b}_0 \left[\frac{1}{3} W\left(\frac{3\mathrm{Ke}^{-6}}{64\, c^{18}} \right) \right]^{1/6}, \tag{B16}$$

where the (earlier mentioned) computed values are $\hat{b}_0 = 1.123$ and $c = 0.80$. The formal difference one could notice between Eq. (B16) and the corresponding result of Ref. [28][8] can be traced back to the omission of the algebraic prefactor $x^{1/6}$ in their counterpart of our Eq. (B5),[12] apart from the exclusion of c in their counterpart of our Eq. (B9). However, in reality, these differences do not affect the leading-order approximation as such, but rather already pertain to a logarithmic correction. Estimating Eq. (B16) at $\mathrm{Ke} = 0.001$ and $\mathrm{Ke} = 0.0001$ yields $\vartheta_{\mathrm{mic}} = 1.72$ and $\vartheta_{\mathrm{mic}} = 1.81$, respectively. These can be compared to (cf. Fig. 9) $\vartheta_{\mathrm{mic}} = 1.67$ and $\vartheta_{\mathrm{mic}} = 1.76$ resulting from Ref. [28] and to $\vartheta_{\mathrm{mic}} = 2.02$ and $\vartheta_{\mathrm{mic}} = 2.07$ resulting from the numerical computation of the full problem. Thus, the result given by Eq. (B16) presents only a minor improvement over the one of Ref. [28] and still appreciably underpredicts the full numerical one. To finalize the calculation of the $O(\zeta)$ correction, we now proceed to the outer region.

3. Outer region and the asymptotic result for ϑ_{mic} including the correction

The corner region is narrow ($\Delta x/\ell_1 \ll 1$), and the evaporation flux is essentially represented by its Taylor expansion about the point $x = \ell_1$, cf. the last terms on the left-hand sides of Eqs. (B13) and (B14). In contrast, the outer region is the one where the flux varies by the order of itself to the right of $x = \ell_1$. Therefore, its longitudinal scale is obviously represented by ℓ_1. Furthermore, in view of the behavior given by Eq. (B15), which now essentially becomes a matching condition, the film slope in the outer region remains of the same asymptotic order as in the corner region (viz. $\hat{\epsilon}$). Thus, the following variables (with a tilde) are appropriate in the outer region:

$$x = \ell_1(1 + \tilde{x}),\ h = \hat{\epsilon}\ell_1\tilde{h} \quad \text{or} \quad \tilde{x} = \zeta\,\hat{x},\ \tilde{h} = \zeta\,\hat{h}, \tag{B17}$$

where two equivalent representations are provided for future convenience. Using the first two Eq. (B17) in Eq. (32) with $J = 2x^{1/2} - \frac{1}{6}x^{-1}$ and only keeping terms up to and including the order $O(\zeta)$, one arrives at

$$\tilde{h}^3 \frac{d^3\tilde{h}}{d\tilde{x}^3} + \zeta(1 + \tilde{x})^{1/2} = 0. \tag{B18}$$

The solution is sought in the form

$$\tilde{h} = \tilde{b}_0\tilde{x} + \zeta\,\tilde{h}_1, \tag{B19}$$

Here the leading-order term is already compatible with both Eq. (33) and the matching condition symbolically written as $\zeta\hat{h}|_{\hat{x}\to+\infty} \sim \tilde{h}|_{\tilde{x}\to 0}$. Furthermore, the latter yields $\tilde{b}_0 = \hat{b}_0\,(= 1.123)$ on account of Eqs. (B12), (B15), and (B17). Thus, the leading-order solution is here just trivial. If one is just bound to the leading order as in Ref. [28], there is no need of introducing the outer region. However, we are here concerned with the first correction, the equation for which is derived upon the substitution of Eq. (B19) into Eq. (B18) as

$$\frac{d^3\tilde{h}_1}{d\tilde{x}^3} = -\frac{(1 + \tilde{x})^{1/2}}{\tilde{b}_0^3\tilde{x}^3}. \tag{B20}$$

Integrating twice and taking into account that $d^2\tilde{h}_1/d\tilde{x}^2 \to 0$ as $\tilde{x} \to +\infty$, one obtains

$$\frac{d\tilde{h}_1}{d\tilde{x}} = \frac{(\tilde{x} - 2)(1 + \tilde{x})^{1/2}}{4\tilde{b}_0^3\tilde{x}} + \frac{4 + \tilde{x}}{8\tilde{b}_0^3} \ln \frac{(1 + \tilde{x})^{1/2} - 1}{(1 + \tilde{x})^{1/2} + 1} + \tilde{b}_1, \tag{B21}$$

where $\tilde{b}_1 = d\tilde{h}_1/d\tilde{x}|_{\tilde{x}\to+\infty}$ is a constant to be determined from matching to the solution in the corner region. From Eq. (B21), one deduces

$$\frac{d\tilde{h}_1}{d\tilde{x}} \sim -\frac{1}{2\tilde{b}_0^3\tilde{x}} + \frac{1}{2\tilde{b}_0^3}\ln\frac{\tilde{x}}{4} + \tilde{b}_1 \quad \text{as} \quad \tilde{x}\to 0. \tag{B22}$$

Then the matching $d\hat{h}/d\hat{x}|_{\hat{x}\to+\infty} \sim d\tilde{h}/d\tilde{x}|_{\tilde{x}\to 0}$, taking into account Eqs. (B12), (B15), (B17), (B19), and (B22), yields

$$\tilde{b}_0 = \hat{b}_0, \quad \tilde{b}_1 = \hat{b}_1 + \frac{1}{2\hat{b}_0^3}\ln\left(\frac{4e}{\zeta}\right) \tag{B23}$$

(the first of these relations was already mentioned before).

Finally, we have $\vartheta_{\rm mic} = dh/dx||_{x\to+\infty} = \hat{\epsilon}d\tilde{h}/d\tilde{x}|_{\hat{x}\to+\infty} = \hat{\epsilon}(\tilde{b}_0 + \zeta\tilde{b}_1)$. Substituting Eq. (B23) into here and rearranging the result in an asymptotically equivalent compact form (valid up to and including the asymptotic order considered on account of $\zeta \ll 1$), one arrives at

$$\vartheta_{\rm mic} = \left[\hat{b}_0^4 + 2\zeta\ln\left(\frac{4}{\zeta}\,e^{1+2\hat{b}_0^3\hat{b}_1}\right)\right]^{1/4}\hat{\epsilon}, \tag{B24}$$

where $\hat{\epsilon}$ and ζ are given by Eq. (B10) while $\hat{b}_0 = 1.123$, $\hat{b}_1 = -0.578$ and $c = 0.80$ are the earlier mentioned computed values. This is the final result of the present Appendix, providing an asymptotic expression for $\vartheta_{\rm mic}$ in the limit Ke $\ll 1$ including the first logarithmic correction. Without the latter, it reduces back to Eq. (B16). It is the result given by Eq. (B24) that is shown in Fig. 9 by the long-dashed line and discussed in Sec. V. We see that accounting for the first logarithmic correction has significantly improved the agreement between the asymptotic theory and the full numerical simulation.

[1] M. Potash and P. C. Wayner, Evaporation from a two-dimensional extended meniscus, Int. J. Heat Mass Transf. **15**, 1851 (1972).

[2] S. Moosman and G. M. Homsy, Evaporating menisci of wetting fluids, J. Colloid Interface Sci. **73**, 212 (1980).

[3] P. C. Stephan and C. A. Busse, Analysis of the heat transfer coefficient of grooved heat pipe evaporator walls, Int. J. Heat Mass Transf. **35**, 383 (1992).

[4] S. DasGupta, I. Y. Kim, and P. C. Wayner, Use of the Kelvin–Clapeyron equation to model an evaporating curved microfilm, J. Heat Transfer **116**, 1007 (1994).

[5] L. M. Hocking, On contact angles in evaporating liquids, Phys. Fluids **7**, 2950 (1995).

[6] S. J. S. Morris, Contact angles for evaporating liquids predicted and compared with existing experiments, J. Fluid Mech. **432**, 1 (2001).

[7] S. J. S. Morris, The evaporating meniscus in a channel, J. Fluid Mech. **494**, 297 (2003).

[8] V. S. Ajaev, Spreading of thin volatile liquid droplets on uniformly heated surfaces, J. Fluid Mech. **528**, 279 (2005).

[9] A. Ye. Rednikov, S. Rossomme, and P. Colinet, Steady microstructure of a contact line for a liquid on a heated surface overlaid with its pure vapor: Parametric study for a classical model, Multiphase Sci. Technol. **21**, 213 (2009).

[10] A. Y. Rednikov and P. Colinet, Vapor-liquid steady meniscus at a superheated wall: Asymptotics in an intermediate zone near the contact line, Microgravity Sci. Technol. **22**, 249 (2010).

[11] A. Ye. Rednikov and P. Colinet, Truncated versus extended microfilms at a vapor–liquid contact line on a heated substrate, Langmuir **27**, 1758 (2011).

[12] P. Colinet and A. Rednikov, On integrable singularities and apparent contact angles within a classical paradigm. Partial and complete wetting regimes with or without phase change, Eur. Phys. J.: Spec. Top. **197**, 89 (2011).
[13] A. Rednikov and P. Colinet, Evaporation-driven contact angles in a pure-vapor atmosphere: The effect of vapor pressure nonuniformity, Math. Model. Nat. Phenom. **7**, 53 (2012).
[14] D. Todorova, U. Thiele, and L. Pismen, The relation of steady evaporating drops fed by an influx and freely evaporating drops, J. Eng. Math. **73**, 17 (2012).
[15] V. Janeček and V. S. Nikolayev, Contact line singularity at partial wetting during evaporation driven by substrate heating, Europhys. Lett. **100**, 14003 (2012).
[16] A. Rednikov and P. Colinet, Singularity-free description of moving contact lines for volatile liquids, Phys. Rev. E **87**, 010401(R) (2013).
[17] V. Janeček and V. S. Nikolayev, Apparent-contact-angle model at partial wetting and evaporation: Impact of surface forces, Phys. Rev. E **87**, 012404 (2013).
[18] V. Janeček, B. Andreotti, D. Pražák, T. Bárta, and V. S. Nikolayev, Moving contact line of a volatile fluid, Phys. Rev. E **88**, 060404(R) (2013).
[19] J. M. Oliver, J. P. Whiteley, M. A. Saxton, D. Vella, V. S. Zubkov, and J. R. King, On contact-line dynamics with mass transfer, Eur. J. Apl. Math. **26**, 1 (2015).
[20] P. Colinet and A. Rednikov, Precursor films and contact line microstructures, in *Droplet Wetting and Evaporation*, edited by D. Brutin (Springer-Verlag, Berlin, 2015).
[21] N. Savva, A. Rednikov, and P. Colinet, Asymptotic analysis of the evaporation dynamics of partially-wetting droplets, J. Fluid Mech. **824**, 574 (2017).
[22] C. Poulard, G. Guéna, A. M. Cazabat, A. Boudaoud, and M. Ben Amar, Rescaling the dynamics of evaporating drops, Langmuir **21**, 8226 (2005).
[23] J. Eggers and L.M. Pismen, Nonlocal description of evaporating drops, Phys. Fluids **22**, 112101 (2010).
[24] C.-T. Pham, G. Berteloot, F. Lequeux, and L. Limat, Dynamics of complete wetting liquid under evaporation, Europhys. Lett. **92**, 54005 (2010).
[25] C.-T. Pham, G. Berteloot, F. Lequeux, and L. Limat, Erratum: Dynamics of complete wetting liquid under evaporation, Europhys. Lett. **93**, 69901 (2011).
[26] C.-T. Pham, F. Lequeux, and L. Limat, Dynamics of a complete wetting liquid under evaporation, in *Without Bounds: A Scientific Canvas of Nonlinearity and Complex Dynamics*, edited by R. G. Rubio, Y.. S. Ryazantsev, V. M. Starov, G.-X. Huang, A. P. Chetverikov, P. Arena, A. A. Nepomnyashchy, A. Ferrus, and E. G. Morozov (Springer-Verlag, Berlin, 2013), pp. 275–283.
[27] F. Doumenc and B. Guerrier, A model coupling the liquid and gas phases for a totally wetting evaporative meniscus, Eur. Phys. J.: Spec. Top. **197**, 281 (2011).
[28] S. J. S. Morris, On the contact region of a diffusion-limited evaporating drop: A local analysis, J. Fluid Mech. **739**, 308 (2014).
[29] E. Jambon-Puillet, O. Carrier, N. Shahidzadeh, D. Brutin, J. Eggers, and D. Bonn, Spreading dynamics and contact angle of completely wetting volatile drops, J. Fluid Mech. **844**, 817 (2018).
[30] J. F. Joanny and P. G. de Gennes, Structure statique des films de mouillage et des lignes de contact, C. R. Acad. Sci. Paris **299 II**, 279 (1984).
[31] H. Hervet and P. G. de Gennes, Dynamique du mouillage: Films précurseurs sur solide sec, C. R. Acad. Sci. Paris **299 II**, 499 (1984).
[32] P. G. de Gennes, Wetting: statics and dynamics, Rev. Mod. Phys. **57**, 827 (1985).
[33] P. G. de Gennes, F. Brochard-Wyart, and D. Quéré, *Capillarity and Wetting Phenomena* (Springer, Berlin, 2004).
[34] C. A. Perazzo, J. R. Mac Intyre, and J. M. Gomba, Analytical solutions for the profile of two-dimensional droplets with finite-length precursor films, Phys. Rev. E **96**, 063109 (2017).
[35] A. Oron, S. H. Davis, and S. G. Bankoff, Long-scale evolution of thin liquid films, Rev. Mod. Phys. **69**, 931 (1997).
[36] A. Ye. Rednikov and P. Colinet, Asymptotic analysis of the contact-line microregion for a perfectly wetting volatile liquid in a pure-vapor atmosphere, Phys. Rev. Fluids **2**, 124006 (2017).

[37] R. D. Deegan, O. Bakajin, T. F. Dupont, G. Huber, S. R. Nagel, and T. A. Witten, Capillary flow as the cause of ring stains from dried liquid drops, Nature **389**, 827 (1997).
[38] Y. O. Popov, Evaporative deposition patterns: Spatial dimensions of the deposit, Phys. Rev. E **71**, 036313 (2005).
[39] R. Marec and J. Straub, Analysis of the evaporation coefficient and the condensation coefficient of water, Int. J. Heat Mass Transfer **44**, 39 (2001).
[40] A. Y. Rednikov and P. Colinet, Contact-line singularities resolved exclusively by the Kelvin effect: volatile liquids in air, J. Fluid Mech. **858**, 881 (2019).
[41] G. Guéna, C. Poulard, and A. M. Cazabat, The leading edge of evaporating droplets, J. Colloid Interface Sci. **312**, 164 (2007).
[42] G. Guéna, P. Allançon, and A. M. Cazabat, Receding contact angle in the situation of complete wetting: Experimental check of a model used for evaporating droplets, Colloids Surf. A **300**, 307 (2007).
[43] Y. Tsoumpas, S. Dehaeck, A. Rednikov, and P. Colinet, Effect of Marangoni flows on the shape of thin sessile droplets evaporating into air, Langmuir **31**, 13334 (2015).